ELSEVIER

Journal of Clinical Imaging 24 (2000) 298–322

CLINICAL IMAGING

MRI of the wrist

Lynne S. Steinbach[a,*], Douglas K. Smith[b,1]

[a]*Muscoloskeletal Imaging, Department of Radiology, 505 Parnassus, Box 0628, University of California San Francisco, San Francisco, CA 94143, USA*

[b]*South Texas Radiology Group, 9150 Huebner, Suite 195, San Antonio, 78240 TX, USA*

Abstract

In the past, the diagnostic imaging algorithm for evaluating the painful wrist included initial plain radiographic examination followed by arthrography, tomography, bone scintigraphy, or computed tomography. In recent years, magnetic resonance imaging (MRI) has been proven efficacious for diagnosing a number of maladies of the bones, ligaments, and soft tissues. MRI can be of aid in evaluation of carpal instability, disorders of the triangular fibrocartilage, ulnar impaction syndrome, distal radioulnar joint (DRUJ) instability, fracture, avascular necrosis (AVN), tendinopathy, nerve entrapment syndromes, synovial abnormalities, and soft tissue masses.

Keywords: Wrist imaging; MRI; Wrist

1. Imaging protocols

We are currently examining patients using a General Electric Signal .5T superconducting magnet (Milwaukee, WI). Most patients are examined using a local receiver coil surrounding the wrist that is placed at the patient's side. Larger patients may need to be examined with their wrist positioned over their head, but this position is less comfortable and tends to be associated with increased motion artifact.

A variety of coils can be used for wrist imaging: (1) paired phased-array circular 3 in. coils, (2) a shoulder coil, or (3) a dedicated wrist coil. It is important for the wrist to be positioned with the dorsum of the hand parallel to the coronal plane of the magnet. Pronation and supination or flexion or extension should be avoided. It may be difficult for patients with wrist pain to maintain this position without adequate immobilization (either using padding or a splint). Adequate padding must be placed between the patient's elbow and the table to improve patient comfort and thereby, to decrease involuntary patient motion. It may be useful to place a pad within the patient's hand against which the fingers can be relaxed to further limit involuntary muscle twitching. The fingers are extended only when we evaluate for carpal tunnel syndrome.

A fast localizer sequence (T1-weighted or gradient echo image) is useful for confirming optimal positioning and to select subsequent imaging sequences. Coronal images should be oriented parallel to the center of the bones of the proximal carpal row (scaphoid, lunate, and triquetrum) (Fig. 1). The alignment of DRUJ should not be used to confirm wrist positioning because of the poor relationship between DRUJ orientation and the orientation of the carpal bones. When imaging the wrist, we use axial images as a guide with cursors aligned parallel and then perpendicular to the proximal carpal row, providing coronal and sagittal images, respectively. An axial scout sequence is followed by coronal T1-weighted and gradient echo 3DFT sequences, an axial T2-weighted fast spin-echo sequence, and a sagittal T1-weighted sequence. In some cases, we will also obtain coronal fast spin-echo images to further evaluate the triangular fibrocartilage and ligaments. The field of view should be as small as possible, ranging from 8 to 10 cm. Although not routinely obtained at our institution, cine motion studies can be performed with fast imaging techniques such as gradient-

* Corresponding author. Tel.: +1-415-353-2062; fax: +1-415-476-8550.

E-mail address: lynne.steinbach@radiology.ucsf.edu (L.S. Steinbach).

[1] Tel.: +1-210-561-7170.

0899-7071/01/$ – see front matter
PII: S0899-7071(00)00218-7

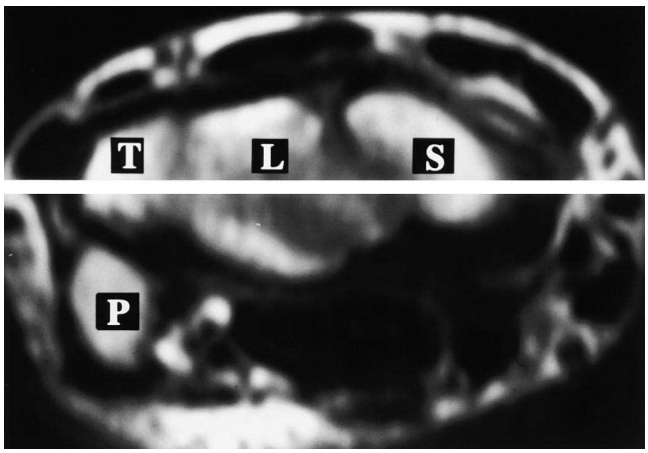

Fig. 1. Axial localizer slice shows proper orientation of wrist. Midportion of bones of proximal carpal row (white line) should be parallel to scan table [scaphoid (S), lunate (L), triquetrum (T), and pisiform (P)]. Pronation or supination of more than 5° should be avoided [4].

echo sequences for evaluation of ligamentous abnormality and carpal instability.

2. Ligamentous disruption and carpal instability

The carpal ligaments are classified as extrinsic and intrinsic ligaments. Extrinsic ligaments originate in the forearm and insert into the carpal bones while intrinsic ligaments originate from and insert into the carpal bones. Most of the extrinsic ligaments abut the wrist capsule and are subclassified by their anatomic location: dorsal or volar.

The dorsal ligament complex is composed of one extrinsic [radiotriquetral ligament (RTL)] and one intrinsic ligament [dorsal intercarpal ligament (DIL)] and is supported by the extensor retinaculum that surrounds the extensor tendons (Fig. 2). The RTL arises from the dorsal radius adjacent to Lister's tubercle and inserts into the dorsal rim of the triquetrum. The RTL is composed of one to three fascicles that may blend with the dorsal capsule of the DRUJ (Fig. 2Bottom left and Right). The DIL is an intrinsic ligament that shares its origin from the dorsal triquetrum with the RTL. The DIL is composed of two fascicles: a triquetroscaphoid fascicle that inserts into the dorsal ridge of the scaphoid and a triquetrotrapezial that inserts on the volar aspect of the triquetrum. Traumatic avulsion of this insertion produces the characteristic curvilinear avulsion fracture that is seen in emergency room. These avulsion fractures typically heal with simple immobilization. Except for the dorsal triquetral avulsion fractures, it is rare to see complete disruptions of the dorsal ligament complex. Patients with dorsal wrist sprains may have soft tissue edema surrounding the dorsal ligaments but there is rarely a visible discontinuity of the dorsal ligaments.

The volar ligament complex is a more complicated structure with eight extrinsic ligaments attaching the carpal bones to the forearm (Fig. 3Previous page, top left). The eight extrinsic ligaments can be considered as three functional groups: (1) three ligaments arising from the styloid process of the distal radius; (2) one to three ligaments arising from volar rim of radius; and (3) two ligaments arising from volar aspect of triangular fibrocartilage. The three ligaments arising from the radial styloid process include the radial collateral ligament (RCL), radioscaphocapitate ligament (RSC), and radiolunotriquetral ligament (RLT; also known as long radiolunate ligament). These three ligaments seem to serve as mechanical guide wires to prevent ulnar translocation of the carpus and to support the scapholunate (SLL) and lunotriquetral (LTL) interosseous ligaments in controlling the motion of the carpal bones. The RLT inserts into the volar portions of the SLL and LTL and has been considered one of the major ligamentous stabilizers of the wrist (Fig. 3Previous page, top right). Disruption of the RLT ligament insertion into the SLL can produce instability of the scapholunate joint (Fig. 3Previous page, bottom).

A group of ligamentous fibers arise from the volar cortex of the distal radius and insert into the proximal pole of the scaphoid [radioscaphoid ligament (RSL)] the scapholunate interosseous ligament [radioscapholunate ligament (RSLL)], which is now thought to represent a neuro-vascular bundle, and volar rim of lunate [radiolunate ligament (RLL)]. Different investigators have considered these fibers different fascicles of one ligament or three separate ligaments. These ligaments appear to play a less important role in stabilizing the carpal bones. We have not been able to appreciate disruptions of these fibers in patients with carpal instability.

The two remaining volar extrinsic ligaments arise from the volar aspect of the triangular fibrocartilage and insert into the volar aspects of the lunate (ulnolunate ligament) and triquetrum (ulnotriquetral ligament) (Fig. 3Above, left). Avulsion fractures of the ulnotriquetral ligament have been recognized. These fractures appear to result from excessive wrist extension with radial deviation (Fig. 3Above, right). These fractures are usually associated with LTL tears and ulnar-sided wrist instability.

Before MRI, little information could be obtained about these ligaments without surgical exploration. On MRI, they are best seen with three-dimensional Fourier transform MRI with multiplanar oblique reconstructions, which allow for images in the planes of the different ligaments [1–3]. MR arthrography is also useful for evaluating these ligaments. Signs of an abnormal ligament on MRI include increased signal intensity on T2-weighting, a segmental defect, increased length, thickening, thinning, and nonvisualization [2]. Both volar and dorsal extrinsic ligaments are usually symmetric between the right and left sides, and therefore, images of the contralateral wrist can be used for comparison purposes in equivocal cases [1,2]. The ligaments are visualized in multiple planes. A wavy contour of the unstressed ligament may be seen in normal individuals. Current experience with MRI for evaluation of disruption of the extrinsic carpal ligaments is limited. Further study

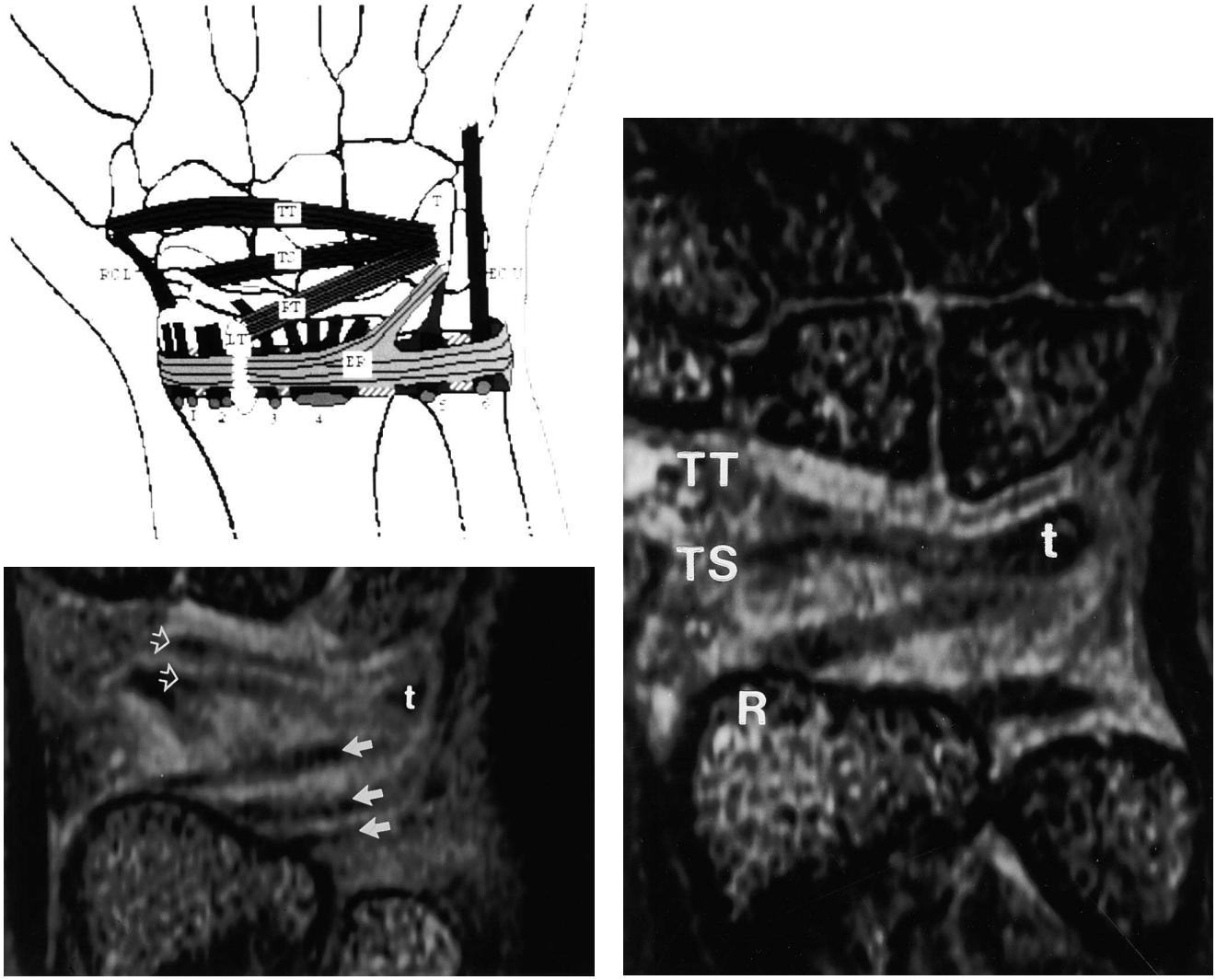

Fig. 2. (Top left) Diagram of dorsal carpal ligaments. Extensor retinaulum (ER) surrounds the six compartments of extensor tendons and extensor carpi ulnaris tendon (ECU) and has attachments to the Lister's tubercle and the triquetrum. Radiotriquetral ligament (LT) is an extrinsic ligament that arises from Lister's tubercle (LT) and inserts into dorsal triquetrum (T). Dorsal intercarpal ligament is an intrinsic ligament with two fascicles: triquetroscaphoid (TS) fascicle inserts in dorsal ridge scaphoid, triquetrotrapezial (TT) fascicle inserts into trapezium along with RCL [1]. (Bottom left) Reconstructed coronal oblique slice through dorsal ligament complex shows single radiotriquetral ligament inserting into triquetrum (t). Triquetroscaphoid (TS) and triquetrotrapezial (TT) fascicles share a common origin from triquetrum and branch proximal to insertions [1]. (Right) Reconstructed coronal oblique slice through dorsal ligament complex shows three fascicles of radiotriquetral ligament and extensor retinaculum and completely separate TS and TT fascicles of dorsal intercarpal ligament.

will be necessary to determine if ligamentous injuries can be diagnosed with MRI.

2.1. Intercarpal ligaments

The two most important intercarpal ligaments are the SLL and LTL. The SLL and LTL are crescent-shaped ligaments with at least three separate anatomic zones [4,5]. The dorsal and volar segments are composed of dense fibrous tissue with strong attachments to the adjacent carpal bones and extrinsic ligaments [6,7]. The central segment of these ligaments is a thin membrane with relatively weak attachments to the adjacent carpal bones. The middle third of the SLL and LTL inserts directly on hyaline cartilage of the scaphoid, lunate, and triquetrum, while volar and dorsal components often insert directly on the carpal bones. The shape and signal characteristics of the interosseous ligaments are variable. The MR appearance of the interosseous ligaments depends upon the plane of imaging and characteristics of imaging sequence. The interosseous ligaments have homogenous black signal using spin-echo imaging sequences but have a more complicated and variable appearance using gradient echo imaging techniques (Fig. 4 Top left and Top right). Smith studied coronal gradient echo images of 80 asymptomatic wrists and reported that the SLL and LTL were visible in all wrists. The SLL was delta-shaped in 90% and linear in 10%. The LTL was delta-shaped in 63% and linear in the remaining. Most of the

ligaments were black or had central intermediate (gray) signal that did not reach the surface of the ligament. Occasionally, intermediate signal was seen traversing the interosseous ligaments (Fig. 4Top left and Top right) but this was distinguishable from a ligament tear because the signal was not as bright as that of fluid (Fig. 4Bottom left and Bottom right). Such a pattern of increased signal intensity on T1 weighting and decreased signal intensity on T2 weighting has been seen with ligament degeneration [8].

Zlatkin et al. [9] proposed three criteria for diagnosing tears of the interosseous ligaments: (1) nonvisualization of the ligament, (2) fluid signal traversing the ligament on T2-weighted images, and (3) morphologic distortion. In Smith and Snearly's [6,7] study of the SLL and LTL in 80 asymptomatic volunteers, fluid signal traversed the interosseous ligaments in only one wrist (one LTL). The shape and signal characteristics of the SLL and LTL were variables with some appearances that could be misinterpreted as a tear [6,7]. Nonvisualization of the interosseous ligaments is a rare manifestation of SLL or LTL tear. Based on shape and signal characteristics, it may be difficult to distinguish a torn ligament from normal variant because of the large range of normal variation. Fluid signal traversing the interosseous ligaments remains a useful sign of ligament perforation or tear (Fig. 4 Bottom left and Bottom right).

Using the criteria listed above, Zlatkin et al. [9] reported accuracies of 90% for diagnosing tears of the SLL and 80% for diagnosing LTL tears using MRI. Most subsequent studies have shown lower sensitivities in the range of 50–70% and specificities of 80–90% [10]. In more recent studies, Totterman et al. [3] demonstrated improved visualization of the intrinsic wrist ligaments using three-dimensional Fourier transform MRI with a custom-designed wrist coil, and Smith and Snearly [6,7] showed that these ligaments could be well seen in asymptomatic individuals using dual echo gradient echo sequences with a dedicated linear, transmit–receive wrist coil.

We have found that fast spin-echo imaging with fat suppression or fast inversion recovery images in the coronal plane are most useful for determining if fluid signal traverses the SLL or LTL (Fig. 4Bottom left and Bottom right). Recently, we have added fast spin-echo images without fat suppression or gradient echo images in the axial plane to evaluate if fluid signal traverses the interface between the interosseous ligaments and the supporting capsular ligaments (confluence zone). We have noticed that patients with clinical wrist instability frequently have tears involving the confluence zone. Perforations of the central segment of the interosseous ligaments are part of the aging process and may not produce any symptoms or instability. The presence of a joint effusion increases the sensitivity of MR images for the interosseous ligaments. Smith [11] has shown increased sensitivity for diagnosing interosseous ligament tears using MRI following conventional carpal arthrography. Three-dimensional Fourier transform gradient-echo techniques provide extremely thin slices that can be loaded as a volume and interactively viewed to optimize visualization of the interosseous and extrinsic ligaments. Although not routinely used, the wrist can also be studied in various positions with MRI (ulnar and radial deviation, flexion and extension) when there is suspected ligamentous disruption or carpal instability [12].

3. Disorders of the triangular fibrocartilage

The triangular fibrocartilage is an important structure that cushions the ulnocarpal and stabilizes the DRUJ. Tears of the triangular fibrocartilage result in nonspecific pain, crepitus, and weakness that can be difficult to distinguish from injuries to the LTL, extensor carpi ulnaris tendon, pisotriquetral, or DRUJs [13,14]. Diagnostic imaging is usually performed in these patients since clinical examination may not give a precise diagnosis for ulnar wrist pain.

Palmer and Werner [15] have defined the triangular fibrocartilage complex (TFCC) as a composite of five structures: (1) the triangular fibrocartilage (also referred to as the "articular disc") and its two dorsal and volar capsular reinforcements (the volar and dorsal distal radioulnar ligaments); (2) the ulnocarpal meniscus, not always identified in the human wrist; (3) the ulnocarpal ligaments, which add stability to the ulnar aspect of the midcarpal joint; (4) the ulnar collateral ligament, which extends from the base of the ulnar styloid to the carpus; and (5) the sheath of the extensor carpi ulnaris tendon, which inserts along the dorsal margin of the base of the fifth metacarpal (Fig. 5).

The triangular fibrocartilage frequently undergoes degeneration, which is often asymptomatic. Degeneration has been demonstrated on histologic studies with increasing prevalence in older individuals. In the first two decades of life, no degenerative changes were detected in Mikic's anatomic study of 180 wrist joints from 100 cadavers. Such changes were seen in 38% and 55% of individuals in the third and fourth decades of life, respectively, and in up to 100% of individuals during the sixth decade [16]. More than 40% of those wrists had perforations of the triangular fibrocartilage.

Degeneration tends to be more severe on the proximal surface due to more intensive biomechanical forces on this surface [15,16]. Progressive degeneration of the proximal surface leads to erosion, thinning, and perforation of the triangular fibrocartilage. Degenerative perforations are more common in the thinner central portion of the triangular fibrocartilage, whereas traumatic tears tend to occur in the radial portion [17].

Arthrography has been useful for excluding complete tears of the triangular fibrocartilage. Tears are indicated by leakage of contrast between the two compartments, which are normally anatomically separated from each other by the triangular fibrocartilage — the radiocarpal joint and the DRUJ. The normal arthrogram demonstrates a lack of

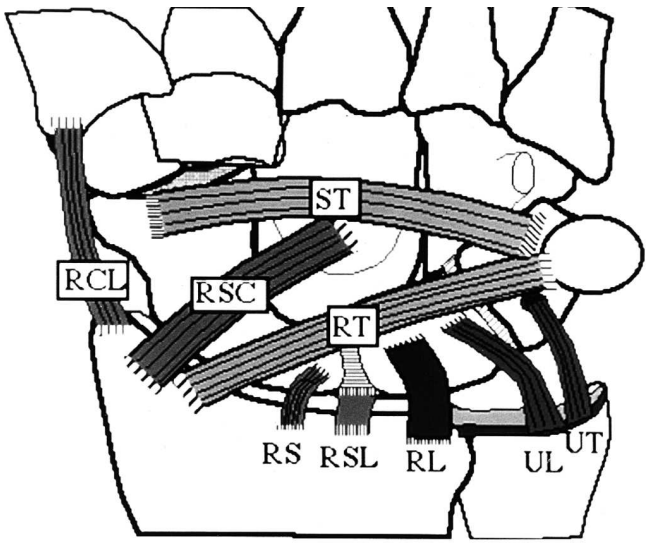
ST
RCL
RSC
RT
RS
RSL
RL
UL
UT

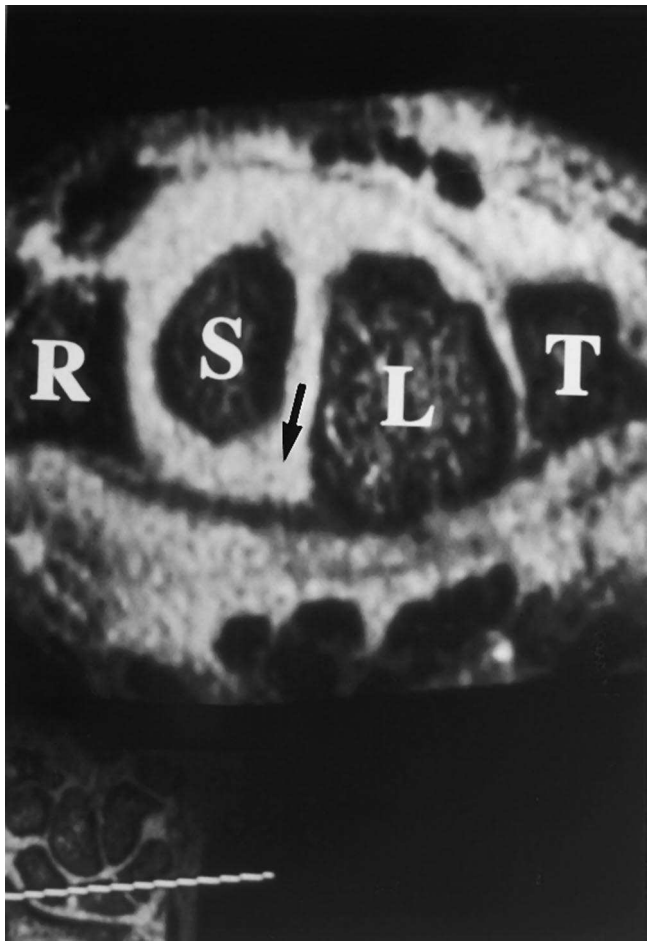
R
S
L
T

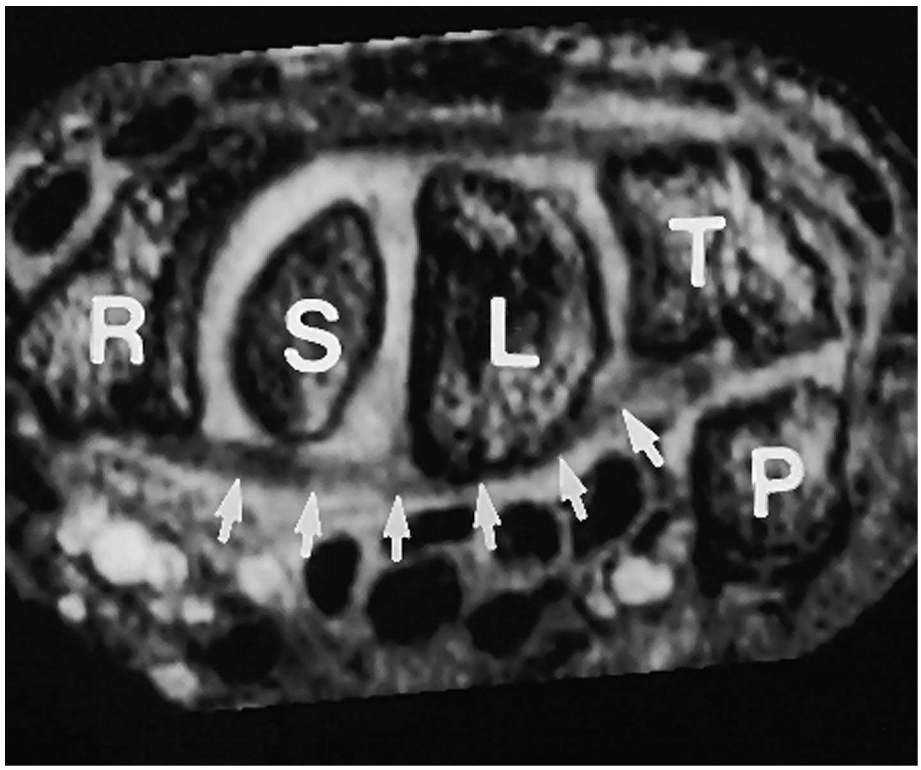
R
S
L
T
P

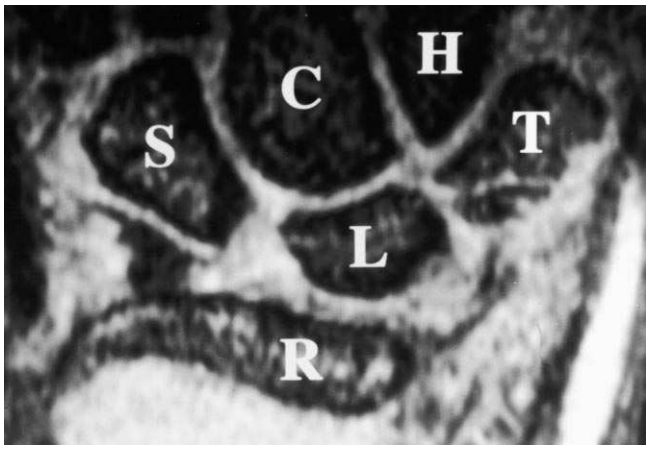

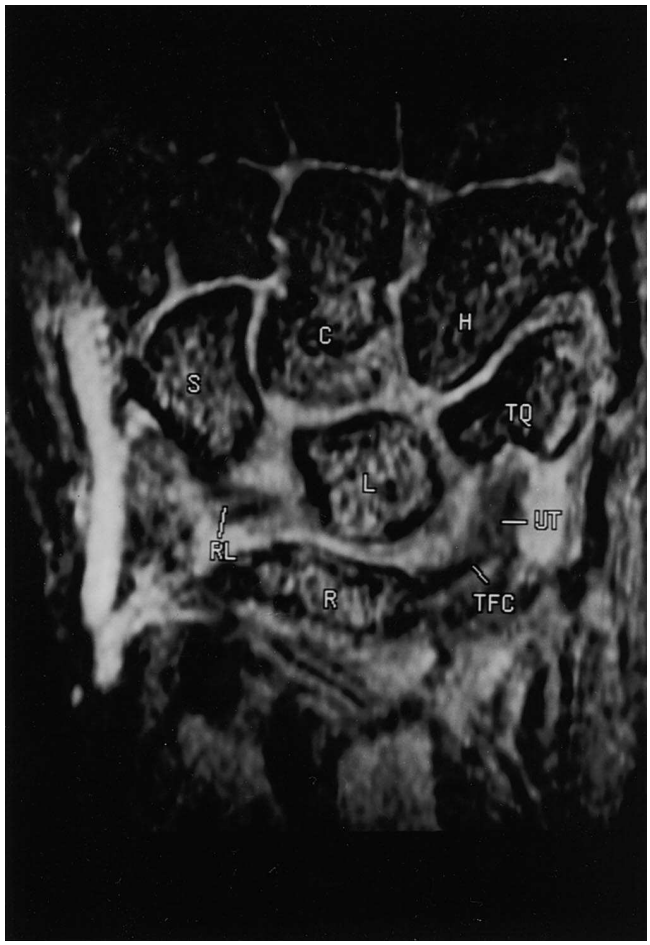

Fig. 3. (Previous page, top left) Diagram of volar carpal ligaments. Three ligaments arise from radial styloid: radial collateral ligament (RCL), radioscaphocapitate (RSC) ligament, and radiolunotriquetral (RLT) ligament. Up to three ligaments have been described arising from volar rim of radius: radioscaphoid (RS), radioscapholunate (RSL), now thought to be a neurovascular bundle rather than a ligament and radiolunate (RL) ligaments. Two ligaments attach triangular fibrocartilage (TFC) to the lunate (ulnolunate ligament — ULL) and triquetrum (ulnotriquetral ligament — UTL). Triquetroscaphoid ligament attaches triquetrum to distal pole of scaphoid [3]. (Previous page, top right) Axial oblique slice through normal radiolunotriquetral (RLT) ligament (arrows) shows origin from radial styloid and attachment into volar poles of lunate and triquetrum [1]. (Previous page, bottom) Axial oblique slice shows disruption of attachment of RLT into volar third of SL ligament and dorsal displacement of scaphoid in patient with scapholunate (dissociative) instability [4]. (Above, left) Coronal gradient echo image shows normal appearance of ulnotriquetral ligament (UT) originating from triangular fibrocartilage (TFC). RL = radiolunate fibers of RLT ligament. S = scaphoid, L = lunate, C = capitate, H = hamate, TQ = triquetrum. (Above, right) Coronal gradient echo image shows avulsion of ulnotriquetral ligament from volar aspect of triquetrum. Most of these fractures are associated with tears of the lunotriquetral ligament [4].

communication between the radiocarpal joint and DRUJ. Communication may occur however between these wrist compartments in 7–35% of asymptomatic individuals, presumably due to degenerative perforation, producing false-positive arthrograms [18,19]. The prevalence of this finding increases in older individuals. Therefore, a test is needed that can eliminate these false positives. MRI can aid in this distinction, with the potential to separate some of the degenerative from traumatic abnormalities of the triangular fibrocartilage.

MRI has been established as a noninvasive technique, which directly evaluates the entire triangular fibrocartilage [9,20–25]. The triangular fibrocartilage is best seen on coronal images obtained with a field of view between 8 and 12 cm. It is a low signal intensity bow tie-like structure that extends radially from the dorsal ulnar aspect of the lunate fossa where it attaches to the intermediate to high signal intensity hyaline articular cartilage of the radius (Fig. 6). Its ulnar attachments are to the fovea at the base of the radial aspect of the ulnar styloid and to the ulnar styloid process. The ulnar attachment is often obscured by surrounding loose vascular connective tissue, which is of intermediate signal intensity. The prestyloid recess is an extension of the radiocarpal joint that also lies near the ulnar attachment of the triangular fibrocartilage. Fluid in this recess produces increased signal intensity. The low signal intensity dorsal and volar distal radioulnar ligaments are most easily seen on axial images where they extend from the radius to the ulna.

When there is degeneration of the triangular fibrocartilage, MRI demonstrates intermediate signal intensity on

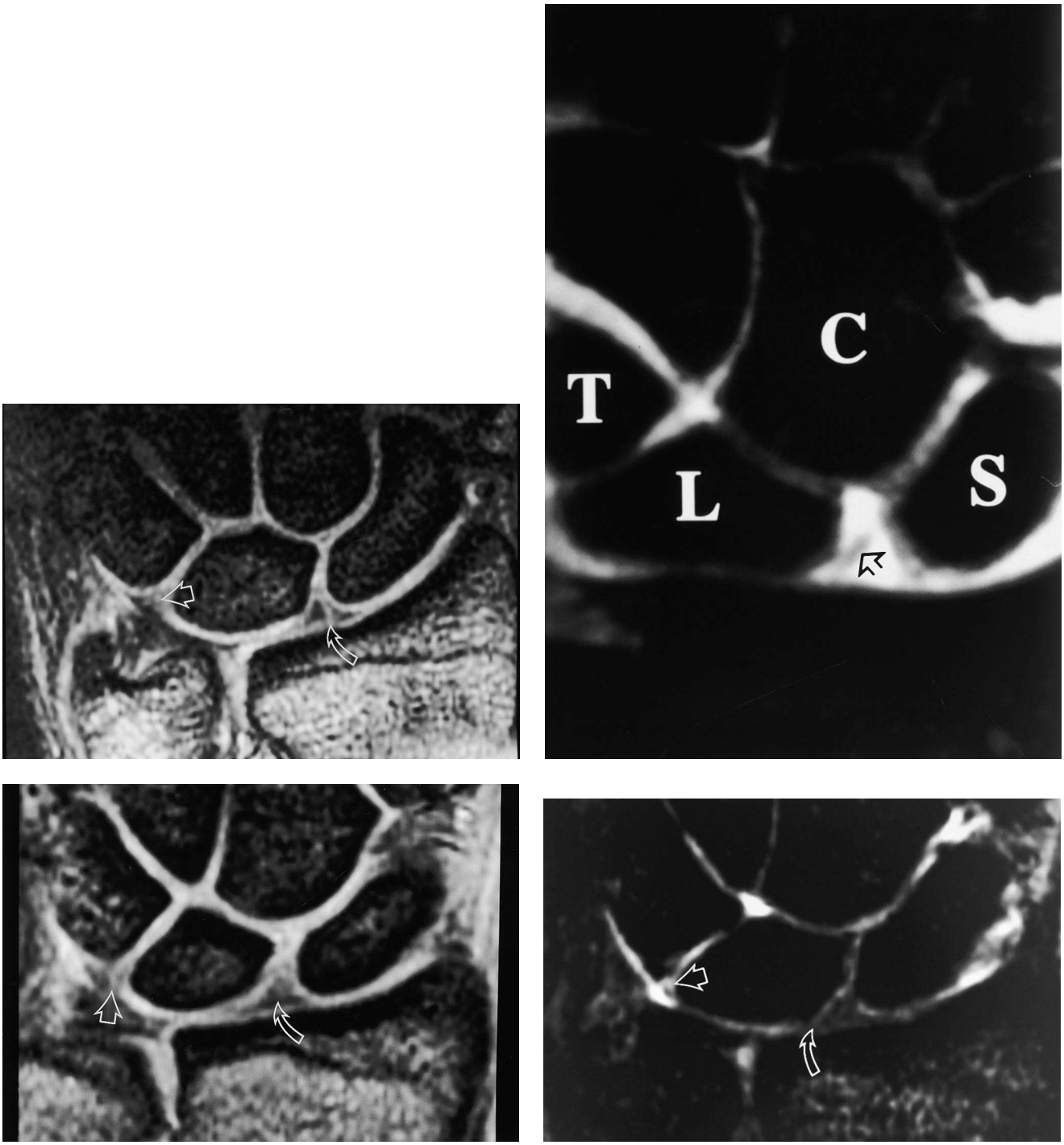

Fig. 4. (Top left) Coronal gradient echo image of volunteer with asymptomatic wrist shows linear intermediate signal traversing scapholunate ligament (curved open arrow). This is normal variant and is not as bright as fluid signal that would indicate tear. Open arrow shows triangular-shaped lunotriquetral ligament with intermediate signal in distal half of ligament. (Bottom left) Coronal fast inversion recovery sequence (TR/TE = 2200/20, TI = 160) of a 24-year-old man following midcarpal arthrogram with dilute gadolinium shows widened scapholunate space and avulsion of scapholunate ligament from scaphoid with ligament stump clearly visible (arrow) [4]. (Top right) Coronal gradient echo image of volunteer with asymptomatic wrist shows linear intermediate signal traversing lunotriquetral ligament (open arrow). This is normal variant and is not as bright as fluid signal that would indicate tear. Curved open arrow shows triangular scapholunate ligament with intermediate signal along insertions into lunate and scaphoid (consistent with hyaline cartilage). (Bottom right) Coronal gradient echo image shows fluid signal traversing lunotriquetral ligament tear (straight open arrow). Curved open arrow shows intermediate signal of hyaline cartilage at site of normal scapholunate ligament insertion [4].

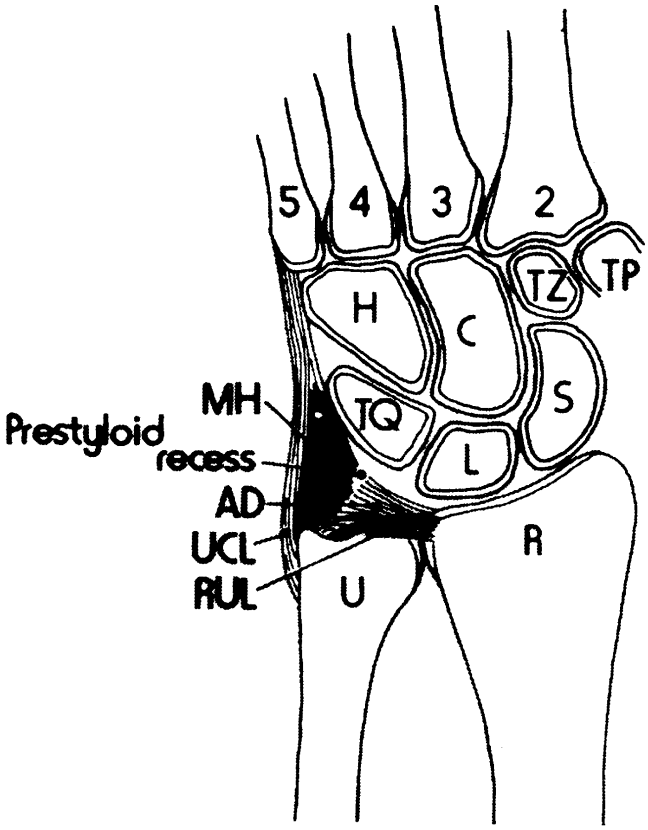

Fig. 5. Diagrammatic representation of some components of the triangular fibrocartilage complex: the ulnocarpal meniscus, also referred to as the meniscus homologue (MH); prestyloid recess; triangular fibrocartilage or "articular disk" (AD); ulnar collateral ligament (UCL); and radioulnar ligaments (RUL). The sheath of the extensor carpi ulnaris tendon is not shown. H = hamate; C = capitate; TZ = trapezoid; TP = trapezium; S = scaphoid; L = lunate; TQ = triquetrum; R = radius; U = ulna [15].

short TE images that does not increase on T2- or T2*-weighted images [8] (Fig. 7). This is believed to be caused by synovial fluid, which diffuses into areas of degeneration and/or an alteration of chemical binding components for "free water" [8,26,27]. Sugimoto et al. [28] reported that high signal intensity was seen in half of the 70 asymptomatic triangular fibrocartilages imaged with spoiled gradient-recalled echo images obtained with the following parameters: TR = 55; TE = 15; 45° flip angle. There was a positive correlation between the high signal intensity, a thin triangular fibrocartilage, and positive ulnar variance. No correlation was seen between high signal intensity in the triangular fibrocartilage and age of the patient.

Perforations of the triangular fibrocartilage can be asymptomatic or posttraumatic and may demonstrate high signal intensity fluid within them on T2-weighted MR images. The asymptomatic perforations and those caused by traumatic tears present as a region of intermediate signal intensity within the triangular fibrocartilage on T1-weighted and proton density spin-echo images. The signal intensity increases on T2-weighted and gradient echo MR images (Figs. 8 and 9). It is imperative that MRI of the triangular fibrocartilage be obtained with some form of T2-weighting to identify these perforations. If complete, the perforation extends to the edges of the fibrocartilage. Some tears are partial and may only extend to the superior or inferior surface. With a traumatic triangular fibrocartilage tear, fluid is usually present in the DRUJ [10]. This finding, however, is not specific for triangular fibrocartilage tear and can be seen in patients with synovitis or mechanical irritation of the DRUJ.

Detection of triangular fibrocartilage tear using MRI has been investigated by Zlatkin et al. [9] who reported a sensitivity of 100% and a specificity of 93% in 41 patients when compared with arthrography; and a sensitivity of 89%, a specificity of 92%, and an accuracy of 90% when compared with arthroscopy and arthrotomy. Another study by Golimbu et al. [22] found a sensitivity of 93% and an accuracy of 95% in 20 patients with surgical correlation. Schweitzer et al. [10] compared MRI with arthrography as a

Fig. 6. Normal triangular fibrocartilage (T1-weighted coronal MR image). The low signal intensity triangular fibrocartilage extends from the intermediate signal intensity hyaline cartilage of the distal radius (arrow) to the ulnar styloid (arrowhead). The margins of the triangular fibrocartilage are smooth [From Chan W, Lang P, Genant H. MRI of the musculoskeletal system. Philadelphia, PA: Saunders, 1994. p. 214. With permission].

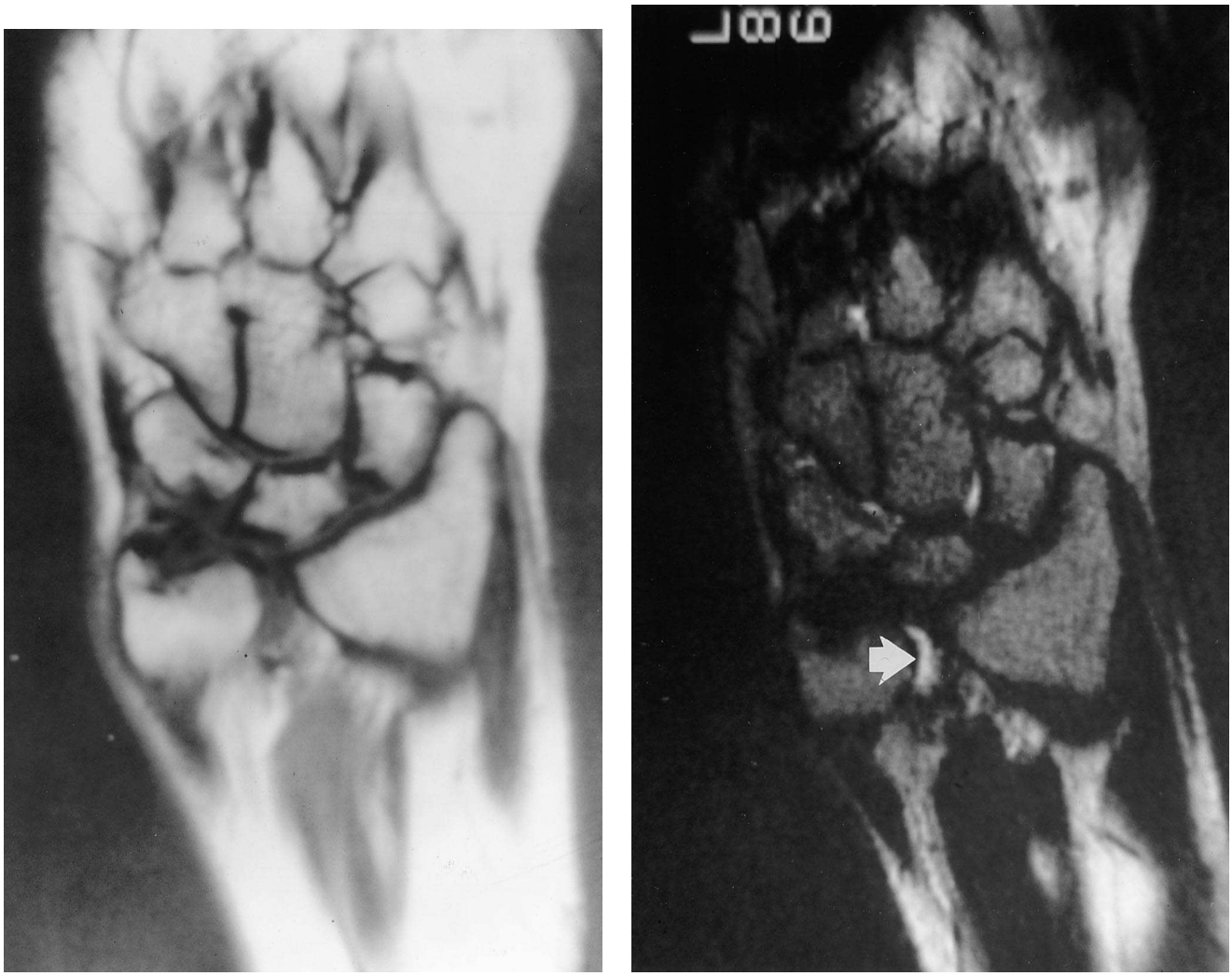

Fig. 7. Degeneration of the triangular fibrocartilage as seen on images obtained from a 0.35-T magnet. (Left) Foci of intermediate signal intensity are present diffusely throughout the triangular fibrocartilage on this coronal proton density MR image. (Right) The entire triangular fibrocartilage is of low signal intensity on the T2-weighted MR image. This pattern is characteristic for degeneration of the triangular fibrocartilage, a finding that was confirmed surgically. Fluid of high signal intensity is seen in the DRUJ, even in the absence of a true tear (arrow), possibly a consequence of overuse [From Chan W, Lang P, Genant H. MRI of the musculoskeletal system. Philadelphia, PA: Saunders, 1994. p. 215. With permission].

gold standard in 15 patients with chronic wrist pain and found MRI to have a 72% sensitivity, 94% specificity, and 89% accuracy. Since the triangular fibrocartilage also stabilizes the DRUJ, triangular fibrocartilage tear is occasionally associated subluxation of the ulnar head, which is well seen on axial MR images (Fig. 10).

4. Ulnar impaction syndrome

The distribution of forces transmitted across the wrist through the radius and ulna is related to the relative lengths of the radius and ulna. In some patients, the ulna is relatively longer than the radius (ulnar positive variance) and results in impaction or abutment of the ulnar head with the lunate during ulnar deviation of the wrist. The MR features of this clinical entity includes ulnar positive variance, subchondral sclerosis or cyst formation of proximal/ulnar aspect of the lunate and/or ulnar head, and tears or perforations of the triangular fibrocartilage and LTL (Fig. 11). In some cases, MRI is able to detect focal defects or signal abnormalities of the articular cartilage of the lunate or ulnar head. In the series by Kang et al. [8], MRI was only able to demonstrate cartilaginous abnormalities in two of the four cadaver wrists with histologically proven erosion of the articular cartilage caused by ulnolunate impaction.

5. DRUJ instability

The DRUJ is formed between the semicircular convex ulnar head and the ulnar concavity in the distal radius

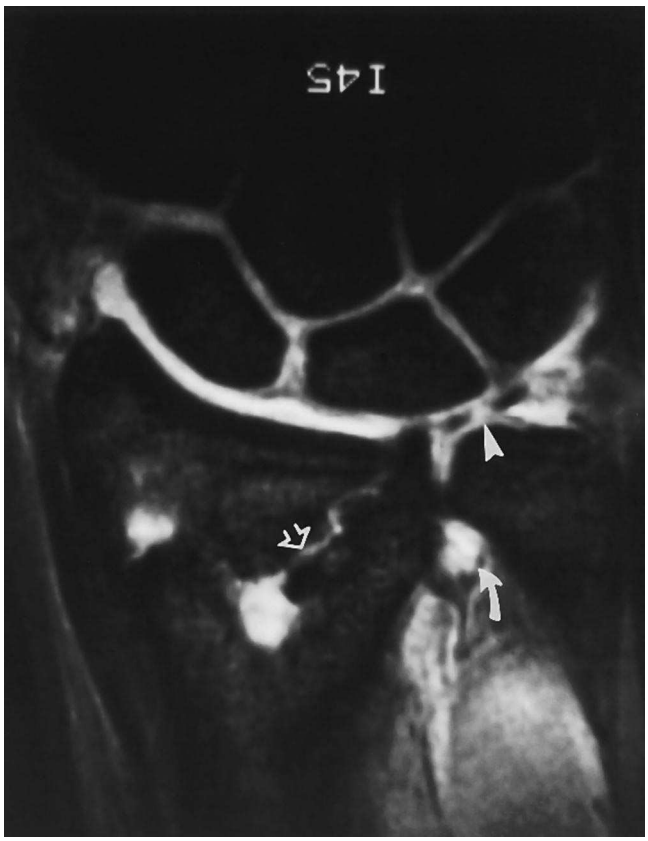

Fig. 8. Triangular fibrocartilage tear associated with a fracture of the distal radius. This coronal gradient echo MR image shows the tear as a high signal intensity gap extending through the full thickness of the triangular fibrocartilage (arrowhead). There is fluid in the distal radiolunar joint (curved arrow). The distal radius fracture is also well seen (open arrow).

— the sigmoid notch. Stability for this joint is provided by the interosseous membrane and to a greater extent by the TFCC.

The diagnosis of DRUJ subluxation can be difficult. Symptoms and physical exam are often nonspecific and conventional radiographs are generally unreliable. Wechsler et al. [29] have described several methods for the diagnosis of DRUJ subluxation by CT which can also be applied to MRI [30] (Fig. 12).

Axial images from both CT and MRI delineate the cross-sectional anatomy of this joint and can be used for evaluating instability (Fig. 13). When evaluating the DRUJ on axial MR images, it is important to be familiar with the small amount of subluxation that can occur with changes in wrist positioning in the normal wrist (Fig. 14). On images of the wrist obtained in neutral position, the distal ulna articulates with the radius in the sigmoid notch. When the wrist is pronated, the ulna moves dorsally, and when the wrist is supinated, the ulnar head moves in a volar direction. When evaluating DRUJ instability, it is optimal to include axial images of both wrists in pronation, supination, and neutral positioning. These images are obtained with the arms above the

Fig. 9. Triangular fibrocartilage tear in a patient with ulnocarpal impaction. The tear is well seen as a high signal intensity gap between the triangular fibrocartilage and the distal radius (black arrow) on this coronal gradient echo MR image. There is a high signal intensity oval lesion in the medial aspect of the lunate, consistent with a cyst (white arrow) created from impaction forces of the distal ulna.

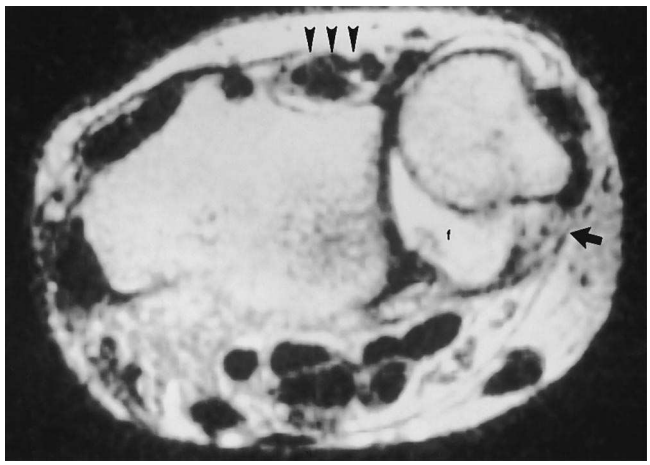

Fig. 10. Dorsal subluxation of the ulna in a patient with rheumatoid arthritis. This woman had a tear of the triangular fibrocartilage, including the volar radioulnar ligament (arrow), a component of the triangular fibrocartilage complex. The tear is high signal intensity on this axial T2-weighted MR image. There is a large amount of fluid in the DRUJ (f) and in the extensor tendon sheath (arrowheads).

patient's head with the wrists placed in a head or neck coil. T1-weighted images provide a fast and accurate method for determination of DRUJ instability. MRI has an advantage for demonstrating soft tissue abnormalities, including triangular fibrocartilage tears, which may be associated with DRUJ instability.

6. Fracture

Although MRI is not routinely used for initial diagnosis of carpal fracture, it can be used for detecting subtle or occult fractures in selected problem cases [31] (Figs. 15 and 16). In most cases, the patient has been immobilized for a

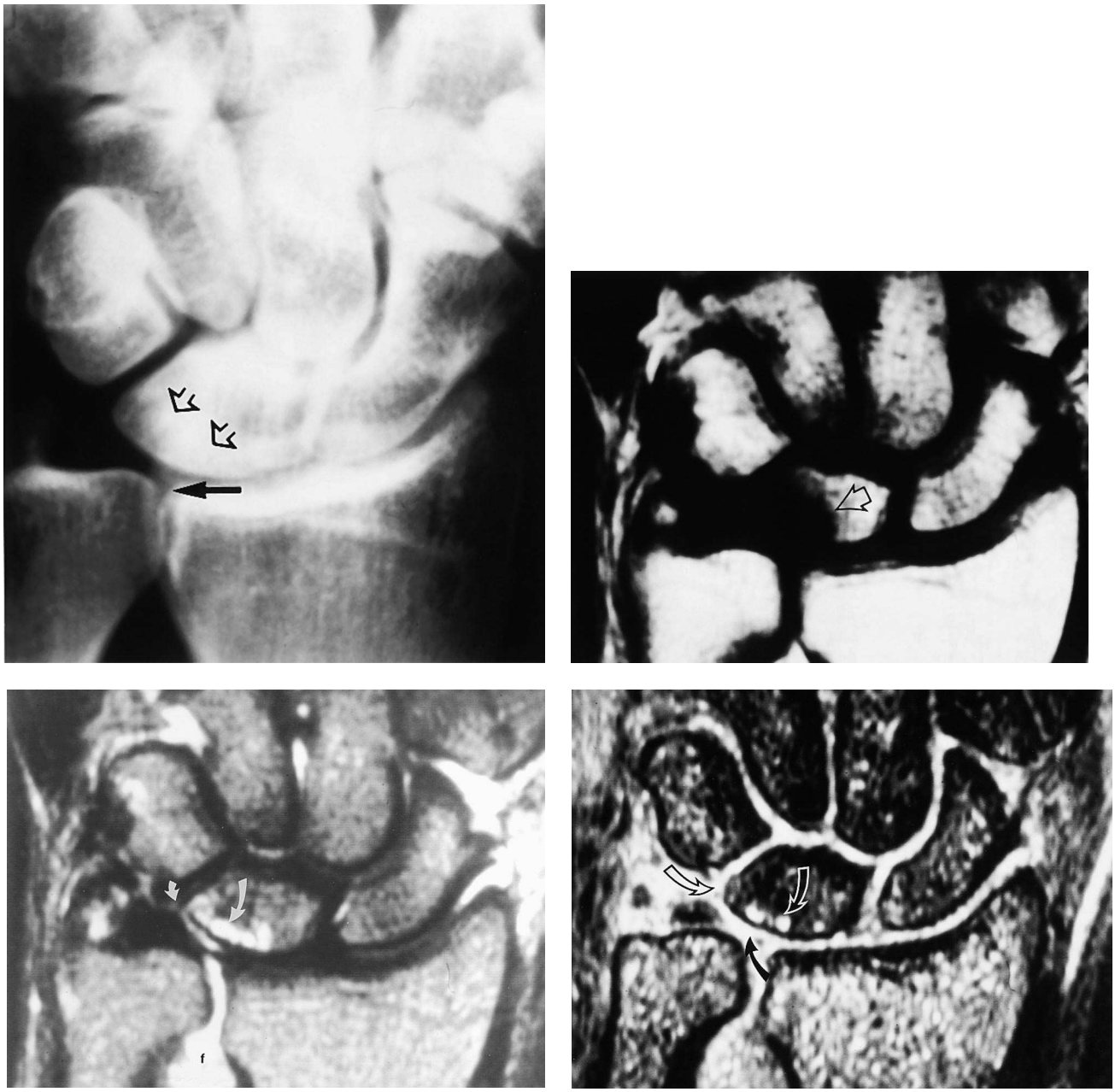

Fig. 11. (Top left) Frontal radiograph of a 30-year-old man shows ulnar head projecting distal to articular surface of radius (closed arrow — ulnar positive variance), subtle sclerosis of proximal/ulnar aspect of lunate (open arrows). (Bottom left) Coronal T1-weighted spin echo image shows ulnar positive variance in patient with ulnocarpal impaction syndrome. Low signal in proximal/ulnar aspect of lunate (open arrow) in area of sclerosis on plain film. (Top right) Coronal fast spin-echo T2-weighted image with fat suppression shows multiple subchondral cysts in lunate (large curved arrow), fluid signal traverses tear of LT ligament (small curved arrow), and there is fluid in the distal radiolunar joint (f). (Bottom right) Three-dimensional gradient echo image shows cysts in proximal aspect of lunate (white open arrow), defect in lunotriquetral ligament (black open arrow), and central defect in triangular fibrocartilage (black curved arrow)

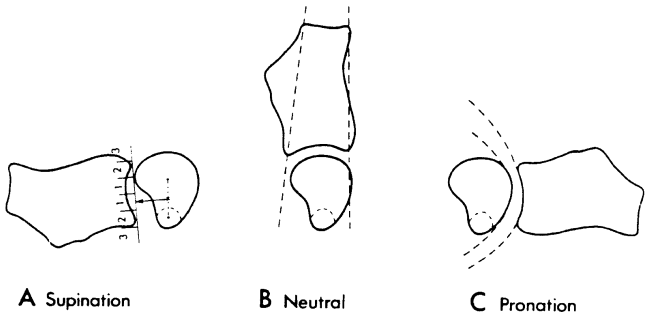

Fig. 12. Methods for assessing radioulnar subluxation. (A) Supination; epicenter method. A perpendicular line is drawn from the center of rotation of the DRUJ (a point halfway between the ulnar styloid process and center of the ulnar head) to the chord of the sigmoid notch. The joint is considered normal if this line is in the middle of the sigmoid notch. The dashed lines represent the location of the styloid process. (B) Neutral; radioulnar line method. Articulation of the ulnar head with the radius is normal if the head falls between the two pictured lines. (C) Pronation congruity method. Note congruity of the arc of the ulnar head with that of the sigmoid notch [29].

week or two and has normal radiographs but persistent pain. In that setting, MR may be useful to distinguish occult fractures that will eventually heal from other entities such as Kienböck's disease that may present with similar features. A fracture is recognizable using MR by the marrow edema (low signal on T1-weighted images and high signal on T2-weighted images) surrounding the fracture line (linear low signal on all sequences) (Figs. 15 and 16). Stress fractures can also be identified using MRI but are uncommon in the wrist [32].

Multipartite carpal bones are not uncommon and can be mistaken for a fracture. The most common site for this is the scaphoid [33]. It may be difficult to distinguish multipartite carpals from true fractures with MRI, except if there is surrounding marrow edema. Therefore, in the absence of surrounding marrow abnormality, a suspected carpal fracture on MRI should be correlated with clinical history and symptoms.

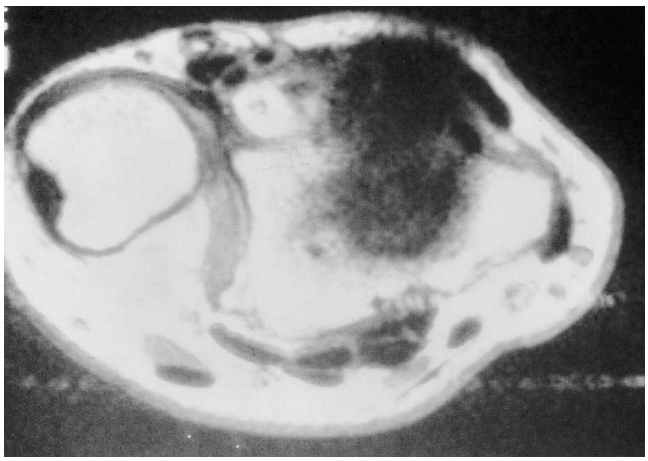

Fig. 13. True dorsal subluxation of the ulnar head associated with a triangular fibrocartilage tear. The volar radiocarpal ligament is absent on this axial T1-weighted MR image [From Chan W, Lang P, Genant H. MRI of the musculoskeletal system. Philadelphia, PA: Saunders, 1994. p. 218. With permission].

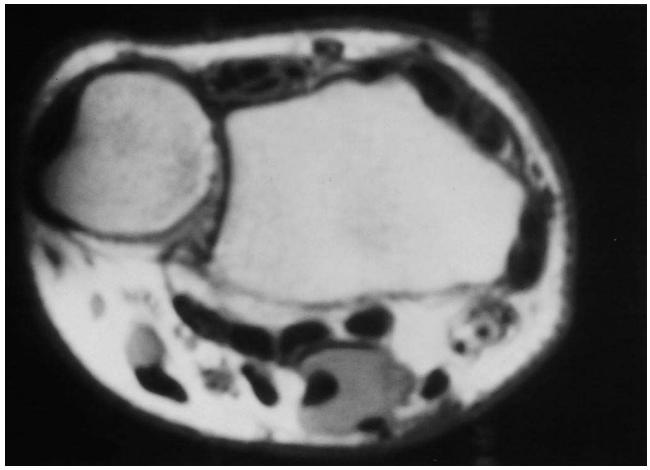

Fig. 14. Pronation of the normal wrist may produce a mild dorsal subluxation of the ulnar head, as demonstrated on this axial T1-weighted MR image [From Chan W, Lang P, Genant H. MRI of the musculoskeletal system. Philadelphia, PA: Saunders, 1994. p. 218. With permission].

7. Avascular necrosis

Idiopathic AVN of the carpal bones usually involves the lunate (Kienböck's disease) or the scaphoid (Preiser's disease) but has been reported in most of the other carpal bones (Fig. 17). MRI is most useful for identifying early carpal bone AVN during the evaluation of a patient with wrist pain of unknown etiology. Plain radiographs are usually normal at this stage and the diagnosis of carpal bone AVN at the time of MR examination is frequently a surprise. MRI is useful for the early diagnosis of carpal AVN [34]. The MR features of carpal bone AVN are replacement of normal fatty marrow with edema (dark on T1WI and bright on T2WI) or fibrosis (dark on both T1WI and T2WI) (Fig. 17). Typically, almost all of the marrow in the carpal bone is involved in contradistinction to more focal processes such as ulnolunate impaction syndrome or fractures. In later stage disease, the involved bone will fragment and lose volume but the diagnosis is usually suspected because of radiographic abnormalities by this late stage. Early diagnosis using MRI is important and useful because most surgical treatments are only successful if they are performed before the involved bone collapses.

7.1. Scaphoid necrosis

Fractures of the scaphoid waist are common injuries and are predisposed to nonunion and posttraumatic AVN of the proximal pole fragment. The nutrient artery for the proximal pole enters the distal scaphoid and must traverse the scaphoid waist. This artery is frequently disrupted with

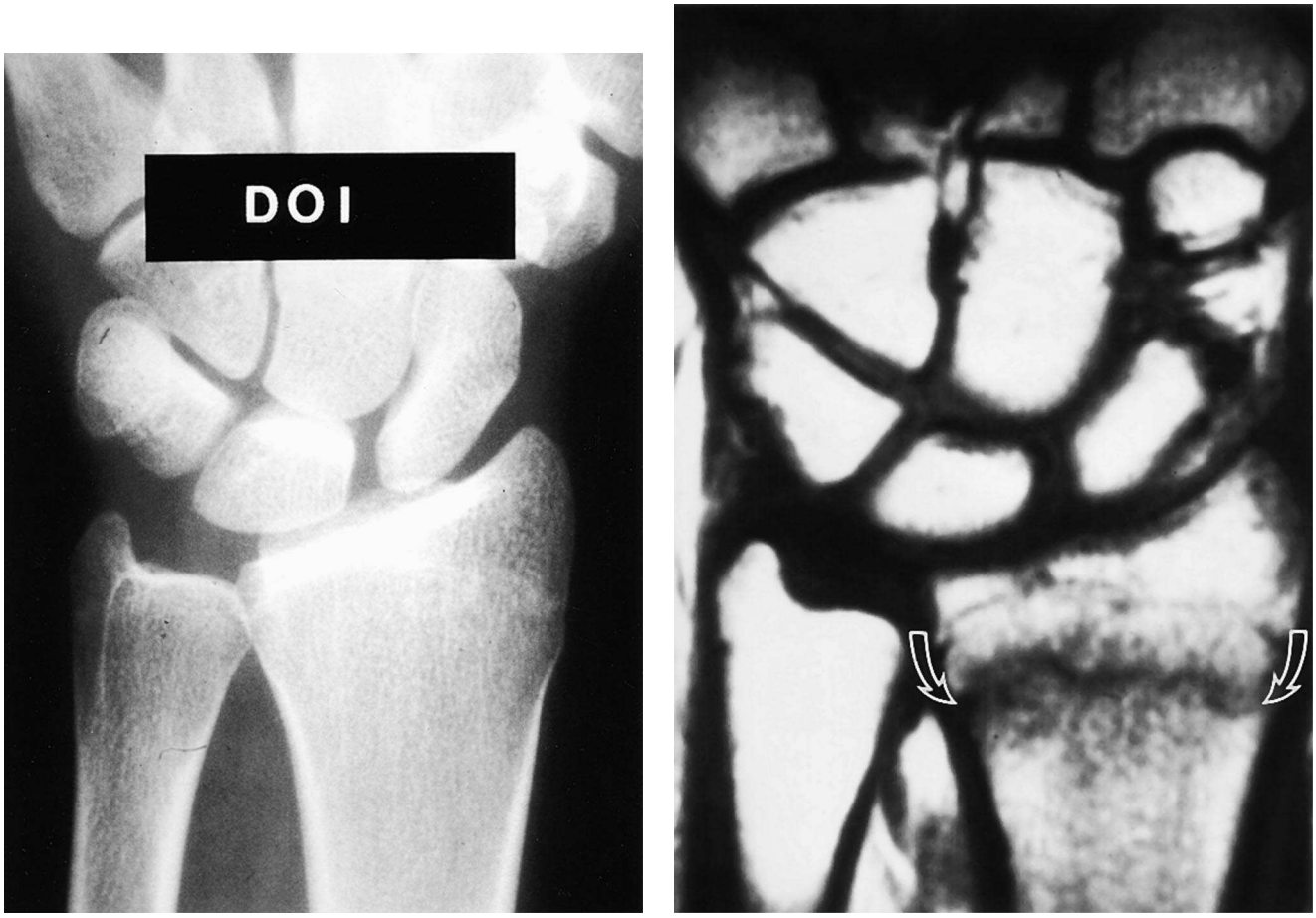

Fig. 15. (Left) Frontal radiograph of young adult on day of wrist injury shows no evidence of fracture. (Right) Coronal T1-weighted spin-echo image obtained 10 days later shows linear black band (fracture line: between arrows) with surrounding intermediate signal (marrow edema) transversing radius in same patient with normal radiograph.

displaced scaphoid waist fractures producing devascularization of part or all of the proximal pole fragment. AVN has been reported in 16% of patients with scaphoid nonunion [35]. If the proximal pole fragment has been devascularized, it is less able to support fracture healing or incorporation of a bone graft [36]. MRI is useful for preoperatively evaluating the vascularity of the proximal pole fragment (Fig. 18). The hand surgeons can test for blood flow intraoperatively but most would prefer to know the vascular status of the proximal pole in order to optimize preoperative planning. AVN can also be seen in the proximal scaphoid in patients without evidence of fracture (Preiser's disease) [37–40].

It can be difficult to detect early AVN in the scaphoid on conventional radiographs and the findings on bone scintigraphy are frequently nonspecific. AVN of the scaphoid is easily detected on coronal MR images [36]. In most cases, there is a transverse band of low signal surrounding the fracture line on T1-weighted coronal images (Fig. 18). The normally bright signal intensity of marrow fat is frequently replaced by low signal intensity after a displaced scaphoid waist fracture or nonunion. This finding suggests previous devascularization with death of fat cells but does not mean that the proximal pole is currently avascular. T2-weighted images with fat suppression usually shows marrow edema surrounding the fracture and including a variable amount of the proximal pole marrow with low signal fibrosis of most of the marrow of the proximal pole fragment. The presence of marrow edema in the proximal pole does not correlate with vascularity.

Early experience of the authors with gadolinium enhanced T1-weighted images has shown that the intensity and quantity of marrow enhancement parallel the intraoperative measures of vascularity (Fig. 18Right). In most cases, there is slightly increased enhancement of the distal pole fragment compared to the other carpal bones. There is intense hyperemia around the fracture nonunion and variable enhancement of the proximal pole fragment. The marrow of a revascularizing proximal pole fragment usually enhances more than surrounding carpal bones. Non-enhancement of the proximal pole fragment indicates absent vascularity and portends a less favorable surgical outcome.

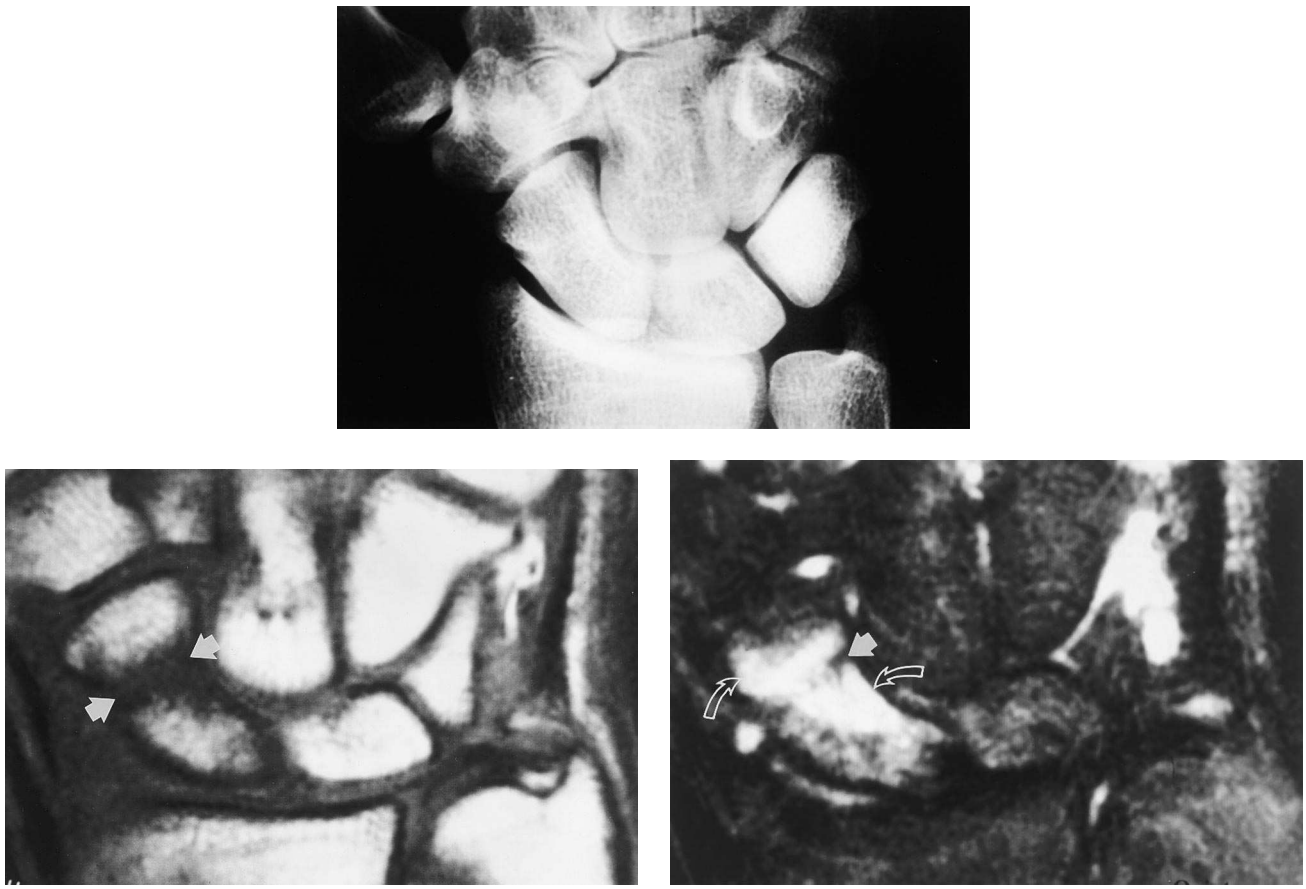

Fig. 16. (Top) Frontal radiograph shows no definite fracture of scaphoid waist. (Left) Coronal T1-weighted spin echo image shows band of low signal intensity surrounding scaphoid waist fracture (between arrows). (Right) Coronal fast spin-echo image with fat suppression shows marrow edema (bright signal: curved arrows) of proximal and distal fragments adjacent to fracture line (dark line: arrow).

7.2. Kienböck's disease

Kienböck's disease (also known as lunatomalacia) refers to AVN of the lunate. It is most common in males 20–40 years of age. Patients usually present with dorsal wrist pain, decreased range of motion of the wrist, and loss of grip strength. The etiology is uncertain although it has been suggested that chronic low-grade trauma is the most important factor. Kienböck's disease is often seen in wrists with negative ulnar variance, where the ulna lies proximal to the distal radius. This configuration is believed to increase shear stress on the lunate, resulting in microfracture and necrosis [41,42].

There are four stages of Kienböck's disease as defined by Lichtman [43]. Stage I represents an early form of Kienböck's disease when radiographs show no evidence of AVN. In this stage, the wrist can be immobilized with reversal of the AVN [44]. In stage II, the lunate is sclerotic without evidence of collapse. Fragmentation and collapse of the lunate are seen in stage III with proximal migration of the capitate, resulting in wrist shortening. This can predispose a patient to scapholunate dissociation with disruption of the SLL as well as carpal tunnel syndrome. In Stage IV Kienböck's disease, the patient develops degenerative changes in the radiocarpal joint as well as subarticular cysts and carpal instability.

In our experience, MRI has been able to demonstrate all stages of Kienböck's disease although it is most useful for diagnosing stage I disease when plain films are negative. In these cases, the patient is usually referred with central wrist pain and negative radiographs. As shown for the scaphoid, the marrow is low in signal intensity on T1 weighting and may have areas of bright T2 signal intensity (marrow edema or neovascularity) and/or areas of dark T2 signal intensity (fibrosis) (Fig. 17) depending on the stage of the disease [45,46].

The finding of focal marrow signal abnormality in the lunate is more frequently seen with other abnormalities than Kienböck's disease (i.e. bone island, osteoid osteoma, intraosseous ganglion or cyst, or ulnocarpal impaction). Correlation of MR findings to conventional radiographs is essential to add specificity to the diagnosis.

Follow-up MR images are useful to monitor treatment of patients with abnormal signal intensity in the lunate suspicious for AVN or bone marrow edema syndrome. Following successful immobilization, the marrow signal intensity may return to normal [47]. There are many different treatments for advanced Kienböck's disease, all having a variable

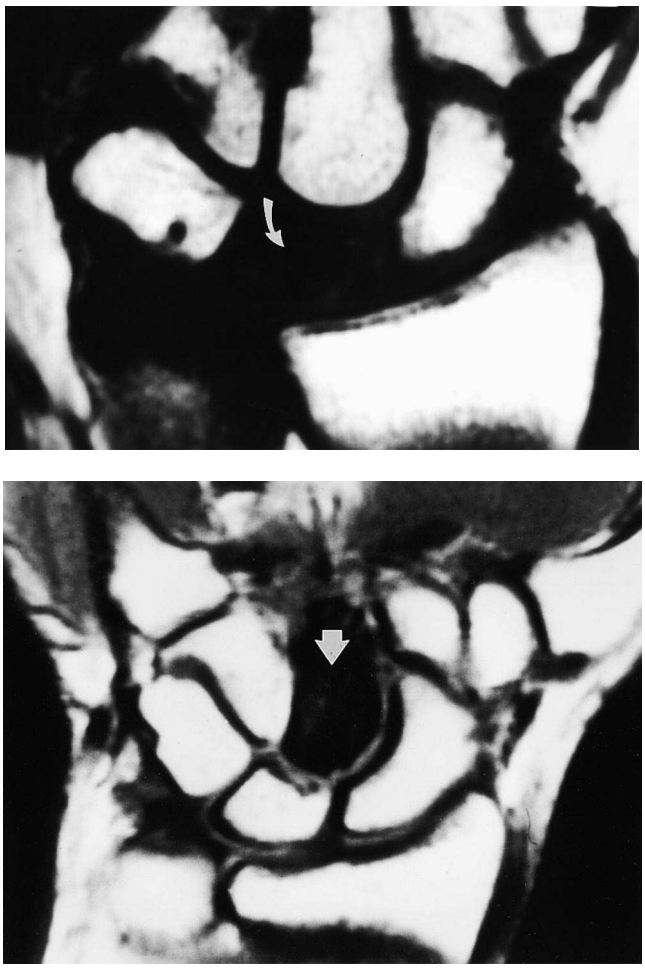

Fig. 17. (Top) T1-weighted coronal image shows uniform black signal replacing bright signal of marrow fat in lunate in patients with Kienbock's disease (curved arrow). (Bottom) T1-weighted coronal image shows uniform black signal replacing bright signal of marrow fat in capitate in patient with AVN (arrow).

success rate. If the lunate is replaced with a spacer such as a rolled tendon or prosthesis, MRI can be used to periodically evaluate spacer position. It can also aid in the identification of prosthesis fracture, displacement, or synovitis when a silastic implant is utilized (Fig. 19).

8. Tendinopathy

The extensor tendons of the wrist are divided into six compartments that overlie the carpal bones and interosseous ligaments along the dorsal aspect of the wrist (Fig. 20). The first compartment lies lateral to the radius and contains the abductor pollicis longus and extensor pollicis brevis tendons. The second compartment, lateral to Lister's tubercle, contains the extensor carpi radialis brevis and longus tendons. The third compartment, located medial to Lister's tubercle, contains the extensor pollicis longus tendon. The fourth compartment contains the extensor indicis proprius and extensor digitorum communis tendons. The extensor digiti minimi lies in the fifth compartment, and the extensor carpi ulnaris is located in the sixth compartment medial to the ulnar styloid. Volar to the palmar ligaments lie the deep and superficial flexor tendons of the digits and the flexor pollicus longus tendon, which traverse the wrist through the carpal tunnel.

Tendinopathy is well seen on MRI. It may be present with fluid in the tendon sheath (tenosynovitis), thickening of the tendon and/or abnormal elevation of signal intensity within the tendon on T1- and/or T2-weighted images (which may be produced by tendinitis or tear), or complete disruption of the tendon (Fig. 21).

When evaluating tendons of the wrist, it is important to keep in mind the magic angle phenomenon, which can be seen in normal tendons if they lie approximately 55° from the direction of the static magnetic field [45]. At this angle, normal anisotropic structures such as tendons may demonstrate intermediate signal intensity on short TE images. Signal intensity observed on short TE images decreases with increasing TE. Thus, increased signal intensity due to the magic angle effect may be misdiagnosed as tendinous degeneration or tendinitis.

Tenosynovitis is seen in both flexor and extensor compartments (Fig. 21). Tenosynovitis in the sheaths of the abductor pollicus longus and extensor pollicus brevis tendons at the level of the radial styloid, De Quervain's syndrome, can be identified with MRI (Fig. 22). A frequent source of pain along the ulnar aspect of the wrist is tenosynovitis of the extensor carpi ulnaris tendon sheath. Subluxation of the extensor carpi ulnaris is also common and can be best demonstrated with the forearm in supination and the wrist ulnarly deviated. Inflammation of flexor tendons within the carpal tunnel is a frequent cause of carpal tunnel syndrome as discussed below.

MRI is useful for demonstrating the presence and extent of tendon rupture, which may be difficult to diagnose clinically [49,50]. This information can also be utilized for planning of tendon repair, relocation, or transfer. Complete tendon ruptures present as a loss of continuity in the low signal tendon. Incomplete ruptures or chronic tears are depicted by MRI as irregular thickening or thinning of the tendon, which may contain areas of high signal intensity on T2-weighted images. Gadolinium takes up in the area of tendon rupture, but is probably not necessary in most cases. Postoperative adhesions and scar tissue around a tendon can lead to functional impairment. MRI can demonstrate the low signal intensity scar tissue around the tendon.

9. Nerve entrapment syndromes

9.1. Carpal tunnel syndrome

Carpal tunnel syndrome, produced when the median nerve is compressed in the wrist, is increasing in frequency with the

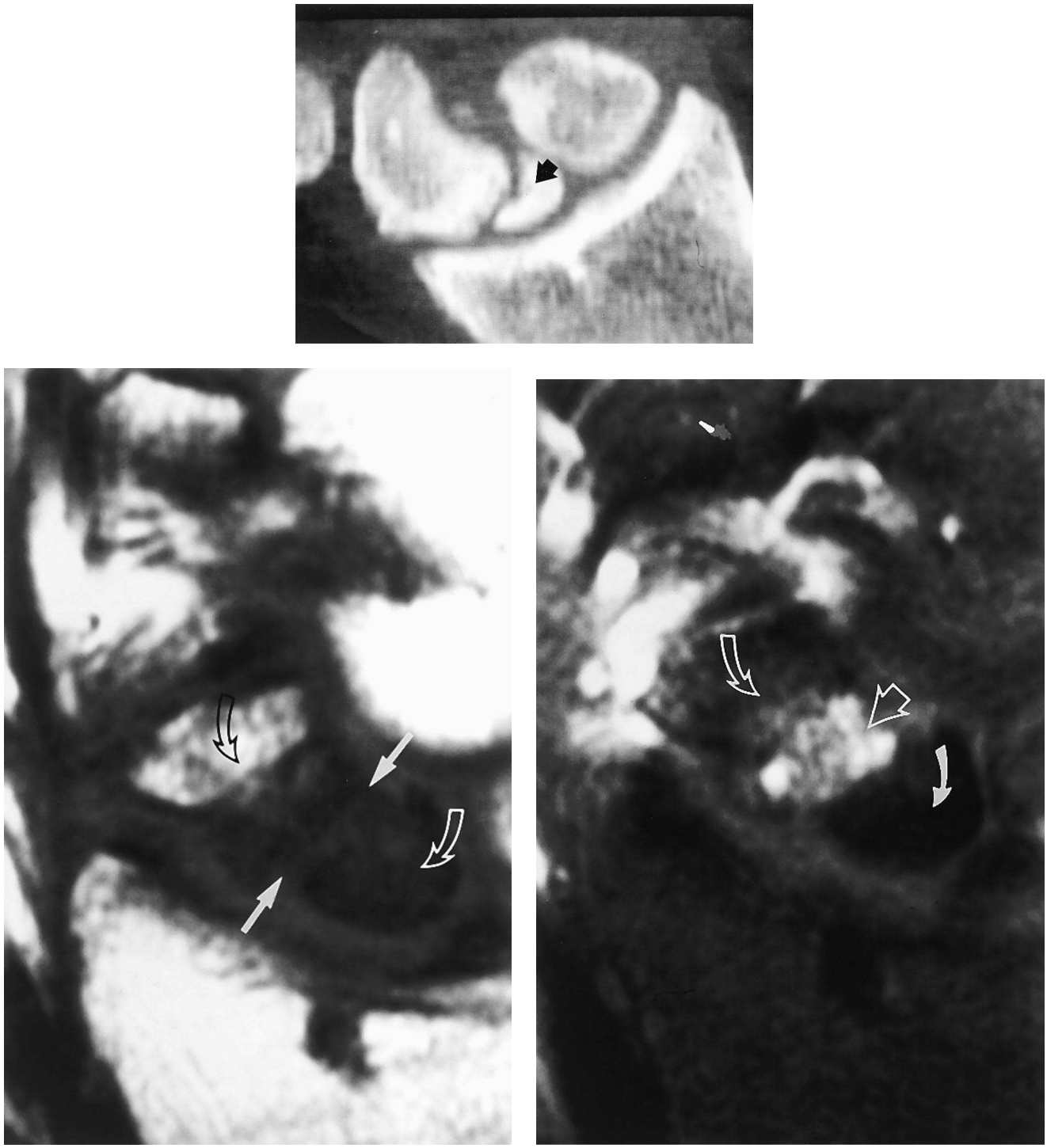

Fig. 18. (Top) CT slice in coronal plane shows proximal pole scaphoid fracture nonunion with relative sclerosis of proximal pole fragment (arrow). (Left) Coronal T1-weighted spin-echo sequence shows intermediate signal traversing scaphoid waist at site of fracture (between solid arrows) with low signal (between curved arrows) adjacent to fracture in distal fragment and involving entire proximal pole fragment (suggesting devascularization). (Right) Gadolinium-enhanced T1-weighted image with fat suppression shows marrow enhancement surrounding fracture (straight arrow), and proximal portion distal fragment (open curved arrow) but no enhancement of devascularized proximal pole fragment (closed curved arrow). The absence of enhancement of the proximal pole correlates with surgical findings and decreases the probability that the nonunion will heal following bone grafting.

increasing number of jobs that require repetitive motion of the wrist. Patients with carpal tunnel syndrome present with pain and tingling of the fingers along the distribution of the median nerve. Most patients with this disorder are 30–50 years of age. Carpal tunnel syndrome is more common in females and is bilateral in up to 50% of cases [51].

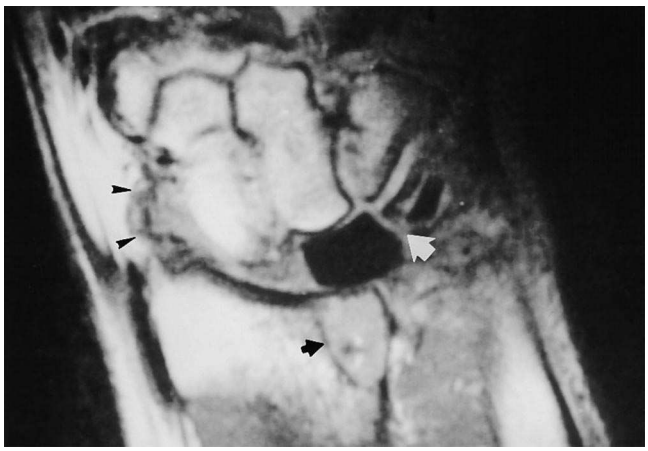

Fig. 19. There is a fracture of the lunate prosthesis (white arrow), which replaces the lunate in a patient with Kienbock's disease. This type of prosthesis is not always visualized on conventional radiographs. The irregularity of the synovium (arrowheads) is suggestive of synovitis, which is commonly seen in patients with a fractured Silastic prosthesis. The patient also had prior carpal fusion, as well as packing of a subcortical distal radial cyst (black arrow) [From Chan W, Lang P, Genant H. MRI of the musculoskeletal system. Philadelphia, PA: Saunders, 1994. p. 222. With permission].

The anatomic causes of median nerve compression can be assessed by MRI. Causes of carpal tunnel syndrome can be divided into two main categories: (1) abnormalities that compress the carpal tunnel from outside such as a mass or malalignment of osseous structures secondary to fracture, Kienböck's disease (Fig. 23), or carpal instability producing abnormal volar narrowing and (2) increased volume within the carpal tunnel caused by inflammation, arthritis, masses, excess fat along the dorsal aspect of the tunnel, persistent median artery, a large adductor pollicus muscle, and edematous and infiltrative disorders. Flexor tenosynovitis and tendinitis resulting from repetitive wrist flexion are the most common causes of carpal tunnel syndrome [52].

MRI is accepted as a useful method for assessment of carpal tunnel syndrome [51,53–55]. The carpal tunnel is bordered inferiorly by the flexor retinaculum, a broad low signal intensity ligament that extends from the hook of the hamate medially to the tuberosities of the scaphoid and

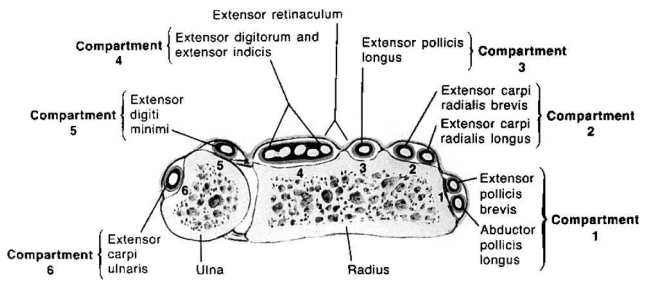

Fig. 20. Extensor tendons of the wrist. Six dorsal tendon compartments are present in the wrist, each with an overlying extensor retinaculum [From Netter F. The Ciba Collection of Medical Illustrations. Summit, NJ: Ciba-Geigy, 1987. With permission].

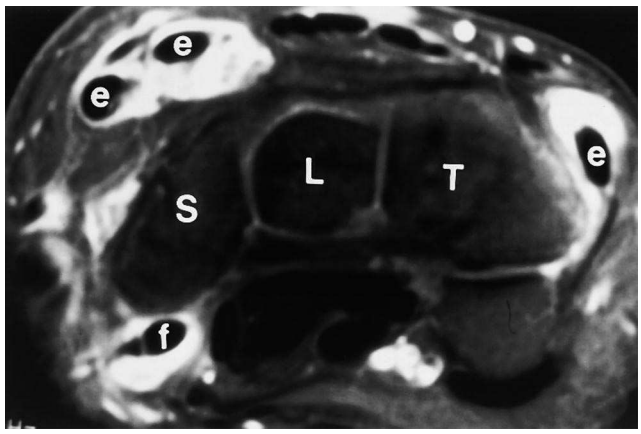

Fig. 21. Axial fat suppressed, fast spin-echo T2-weighted image shows tenosynovitis of multiple tendons in patient with rheumatoid arthritis. Bright signal synovium distending multiple extensor tendon sheaths (e) and flexor carpi radialis tendon sheath (f).

trapezium laterally, holding the flexor tendons in place during wrist flexion (Fig. 24). The rigid roof of the carpal

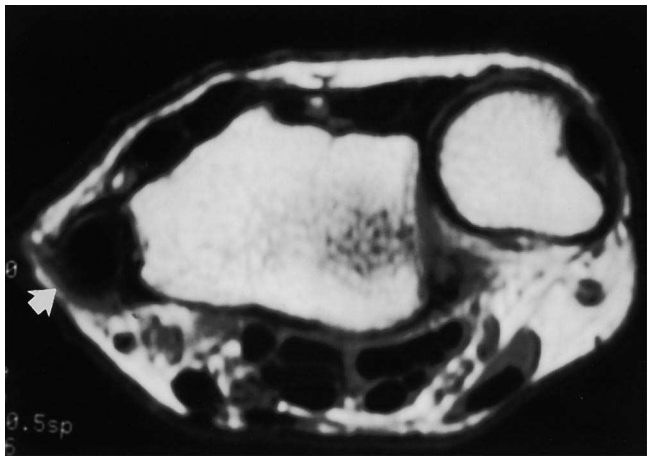

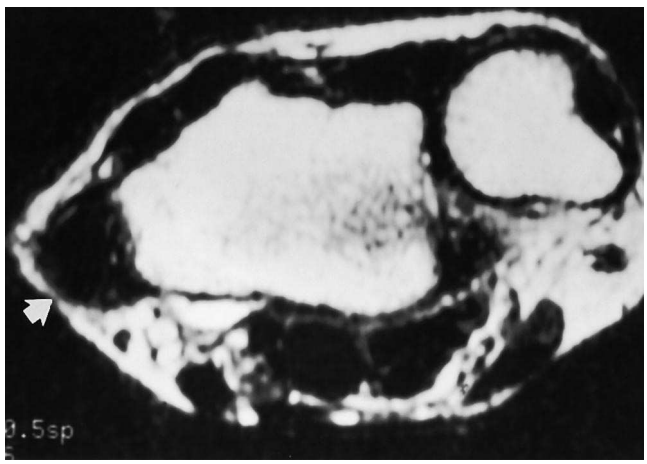

Fig. 22. De Quervain's syndrome. (Top) There is tendinous enlargement with surrounding tenosynovitis in the first extensor compartment (arrow) on this axial T1-weighted image. (Bottom) The compartment is low signal intensity on T2-weighted images as well (arrow), consistent with a stenosing tenosynovitis.

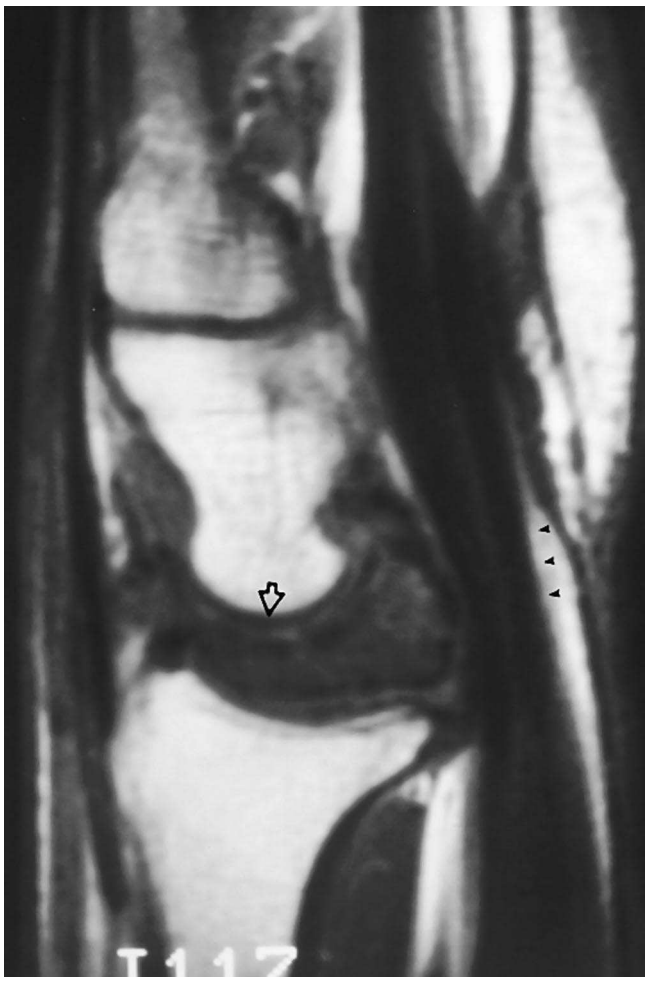

Fig. 23. Kienbock's disease producing carpal tunnel syndrome. T1-weighted MR image demonstrates collapse and volar expansion of the avascular low signal intensity lunate (arrow), with compression of structures in the adjacent carpal tunnel (arrowheads).

tunnel is formed by the carpal bones. The low signal intensity flexor digitorum profundus and flexor digitorum superficialis tendons lie within the tunnel as does the flexor pollicus longus tendon, which lies radial to the other tendons. The tendon sheaths are intermediate signal intensity. There should only be several millimeters of distance between each of the tendons.

The median nerve is easily seen on axial MR images as a rounded or occasionally flattened structure of intermediate signal intensity. The caliber of the median nerve is relatively constant at the level of the DRUJ, pisiform, and hook of the hamate. It is usually located along the superficial radial aspect of the carpal tunnel just deep to the flexor retinaculum and anterior to the superficial flexor tendon of the index finger [53,56]. Occasionally, the nerve can lie deeper in the carpal tunnel, perpendicular to the flexor retinaculum (Fig. 25). Patients with this normal variation are more prone to carpal tunnel syndrome. The position of the nerve can also vary between flexion and extension, and this can be observed with MRI [55]. Flexion of the wrist produces anatomic crowding in the carpal tunnel, seen as flattening or interposition of the nerve between the flexor tendons while wrist extension increases the distance between the median nerve and flexor tendons.

Carpal tunnel abnormalities can be visualized with MRI, however, in our experience, the MRI is not always abnormal in patients with carpal tunnel syndrome. Because of the lack of sensitivity, as well as the expense of MRI, we believe that MRI should be reserved for certain situations. Current clinical applications for MRI of carpal tunnel syndrome include: (1) equivocal cases when the EMG does not correlate with clinical symptoms of carpal tunnel syndrome, (2) identification of the etiology of carpal tunnel syndrome such as an intrinsic or extrinsic mass which may obviate the need for flexor retinaculum release, (3) preoperative assessment of the position of the median nerve in patients who are

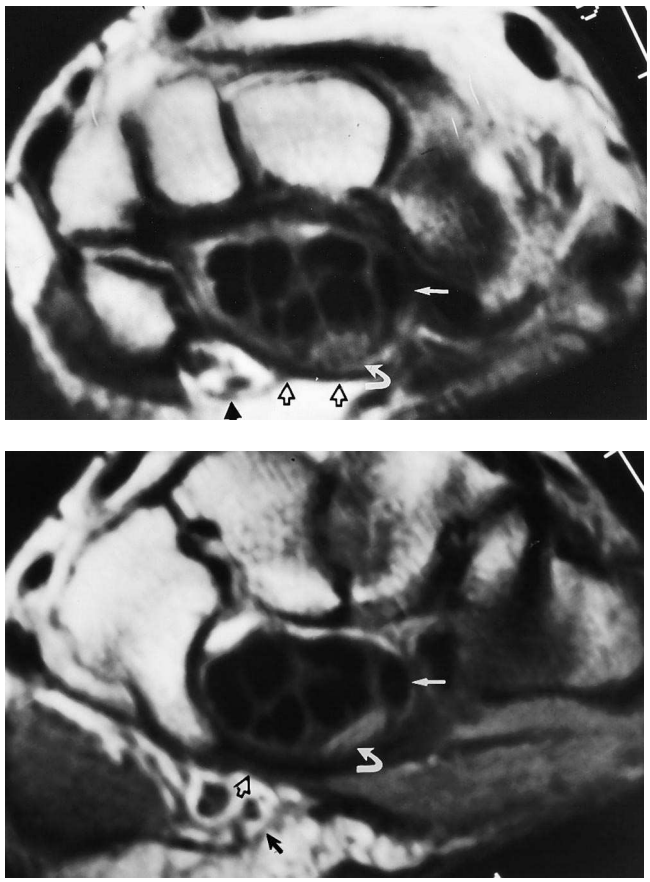

Fig. 24. Normal carpal tunnel on axial T1-weighted MR images obtained at the level of the pisiform (Top) and hamate (Bottom). The carpal tunnel is bordered volarly by the low signal intensity flexor retinaculum (open arrows). The roof of the carpal tunnel consists of the carpal bones and the palmar extrinsic and intrinsic ligaments of the wrist. The flexor digitorum profundus and superficialis tendons, along with the flexor pollicis longus tendon (white arrow), lie within the carpal tunnel. The intermediate signal intensity median nerve usually lies in a radial volar location (curved arrow). The nerve flattens out at the level of the hook of the hamate. Guyon's canal, which contains the ulnar nerve, lies volar to the pisiform and hook of the hamate (solid black arrow).

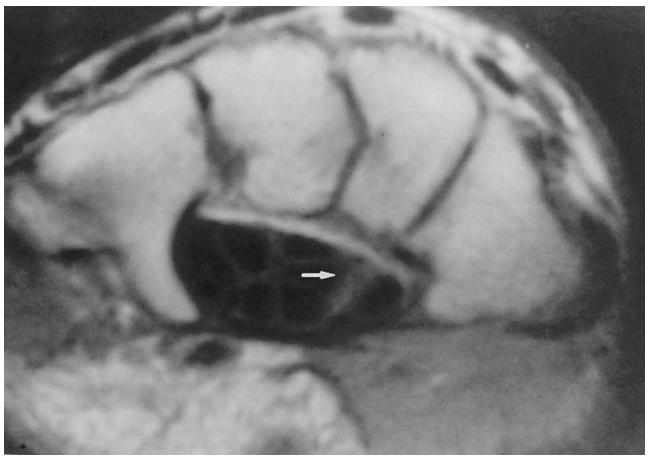

Fig. 25. Normal variant. The median nerve lies deeper in the carpal tunnel (arrow), a location that can predispose to compression [From Chan W, Lang P, Genant H. MRI of the musculoskeletal system. Philadelphia, PA: Saunders, 1994. p. 226. With permission].

scheduled for endoscopic retinacular release, and (4) postoperative assessment of patients whose symptoms recur following surgery.

In cases of tenosynovitis, MR images will demonstrate distention of the tendon sheaths (Fig. 26). In acute tenosynovitis, fluid will be seen within the tendon sheaths on MR images. Tendinitis may present as enlargement and abnormal elevation in signal intensity within the tendon. It is important to exclude the presence of a magic angle phenomenon in tendons that are high signal intensity on short TE images [48]. Tenosynovitis and tendinitis can be localized or diffuse and may be caused by overuse syndromes or an inflammatory arthropathy such as rheumatoid arthritis. Other abnormalities that can be identified by MRI in patients with carpal tunnel syndrome include palmar bowing of the flexor retinaculum (best identified at the level of the hamate), swelling, flattening, or attenuation of the median nerve, and elevated signal intensity within the nerve on T2-

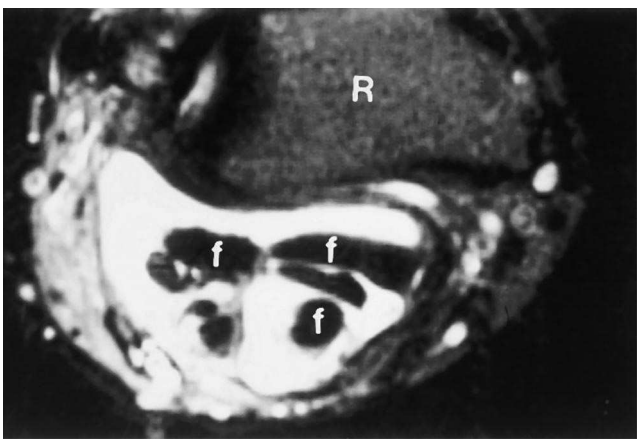

Fig. 26. Axial fat suppressed, fast spin-echo T2-weighted image shows bright signal synovitis in flexor tendon sheaths surrounding flexor tendons (f). R = radius.

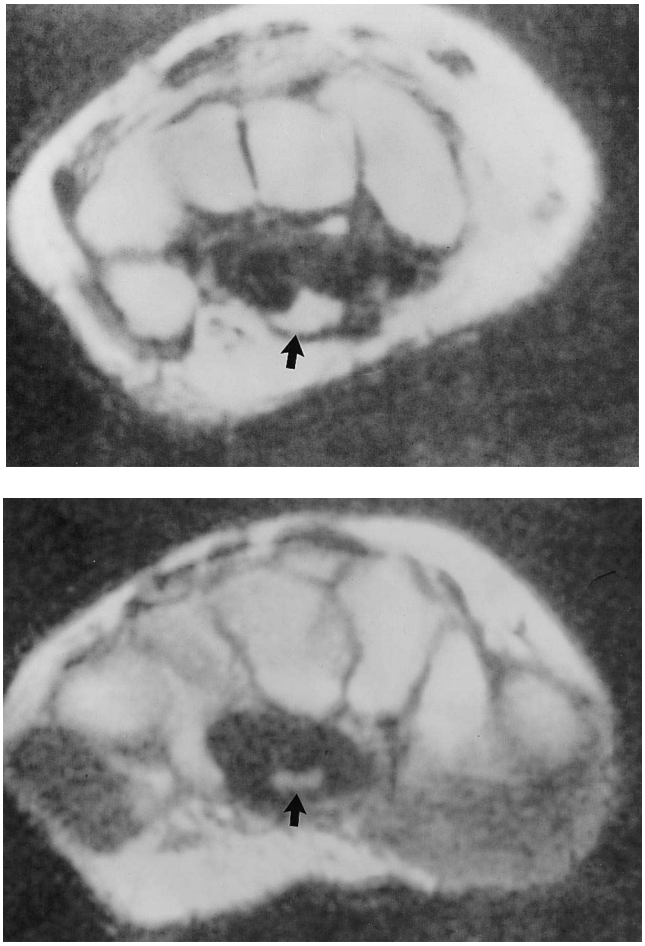

Fig. 27. Carpal tunnel syndrome. T2-weighted axial MR images obtained at the level of the pisiform (Top) and hamate (Bottom). The median nerve is swollen at the level of the pisiform (arrow) but not at the level of the hook of the hamate (arrow). This finding is often seen in patients with carpal tunnel syndrome. The nerve is of high signal intensity, consistent with edema and inflammation. Some degradation of the image has occurred from wrist movement related to pain from carpal tunnel syndrome [From Chan W, Lang P, Genant H. MRI of the musculoskeletal system. Philadelphia, PA: Saunders, 1994. p. 227. With permission].

weighted images, presumably from compression-induced edema [51]. Swelling of the median nerve is often seen proximal to the level of the carpal tunnel at the level of the pisiform (Fig. 27). With long-standing carpal tunnel syndrome, the nerve may have low signal intensity on all imaging sequences, presumably due to fibrosis. Thenar muscle atrophy may also be seen. Occasionally, muscles can hypertrophy within the carpal tunnel, particularly the lumbricals, which lie distally and originate from the flexor digitorum profundus tendons. It is important to keep the fingers extended when evaluating the carpal tunnel to avoid overcalling lumbrical muscle hypertrophy since the lumbrical muscles may slip into the location of the carpal tunnel with finger flexion [54].

Recently, Sugimoto et al. [57] demonstrated two abnormal patterns of enhancement of the median nerve in patients

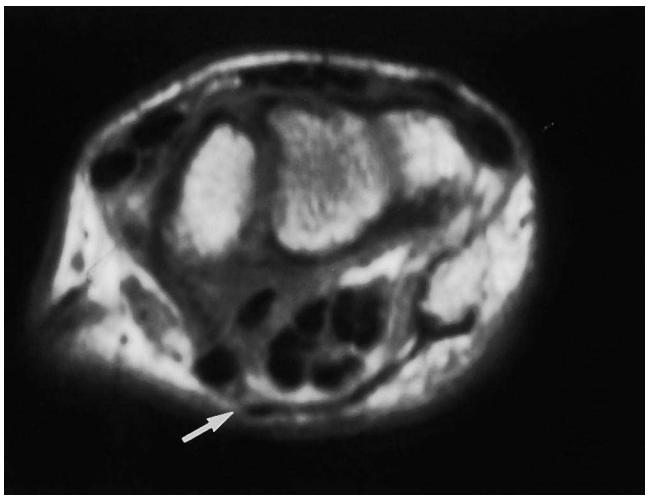

Fig. 28. Normal appearance of the carpal tunnel after release of the flexor retinaculum. The axial T1-weighted image at the level of the pisiform reveals volar displacement of the contents of the carpal tunnel. The flexor retinaculum also is displaced volarly, and is incomplete, with evidence of prior release along the radial aspect (arrow) [From Chan W, Lang P, Genant H. MRI of the musculoskeletal system. Philadelphia, PA: Saunders, 1994. p. 228. With permission].

with carpal tunnel syndrome following intravenous gadolinium administration. Those nerves that demonstrated marked enhancement were postulated to be edematous, while those that did not enhance with contrast were thought to be ischemic. When the wrists with nerves that enhanced were flexed or extended, they often changed their pattern to a lack of enhancement. This change was associated with increase in symptoms of carpal tunnel syndrome. The authors concluded that carpal tunnel syndrome may result from a circulatory disturbance.

Carpal tunnel syndrome is usually treated conservatively with splinting and medication. If symptoms continue despite conservative treatment, the flexor retinaculum is surgically released. This can be done as an open procedure or by blind endoscopic release. Since the endoscopic technique is done with a limited field of the view, the nerve is more prone to injury. Following successful carpal tunnel release, the flexor retinaculum and contents of the carpal tunnel are volarly displaced [58] (Fig. 28). MRI can be utilized following surgical decompression for those patients who are symptomatic to assess for incomplete retinacular release or reattachment, scarring in the region of the carpal tunnel, neuritis of the median nerve, or development of a neuroma, which can occur when the median nerve is inadvertently cut [51] (Fig. 29).

9.2. Guyon's canal syndrome

MRI can reliably demonstrate the area of Guyon's canal [59]. It is in this fascial tunnel that the ulnar nerve enters the palm from the forearm and extends distally from the level of the pisiform where it divides into two sensory branches as well as the deep motor branch. Guyon's canal extends approximately 4 cm from the palmar carpal ligament at the proximal edge of the pisiform to the origin of the hypothenar muscles at the level of the hamate (Fig. 24). Besides the ulnar nerve, the ulnar artery and occasional veins pass through this region and there is abundant adipose tissue surrounding these structures which allows them to be well visualized by MRI.

The deep motor branch of the ulnar nerve is subject to compression by repetitive motion, adjacent masses such as ganglia, lipomas, and anomalous muscles compressing the canal, ulnar artery false aneurysm, hypertrophy of the flexor carpi ulnaris tendon, hypertrophy of the palmar carpal ligament, osteoarthritis of the pisiform–triquetral joint, or fractures at the bases of the

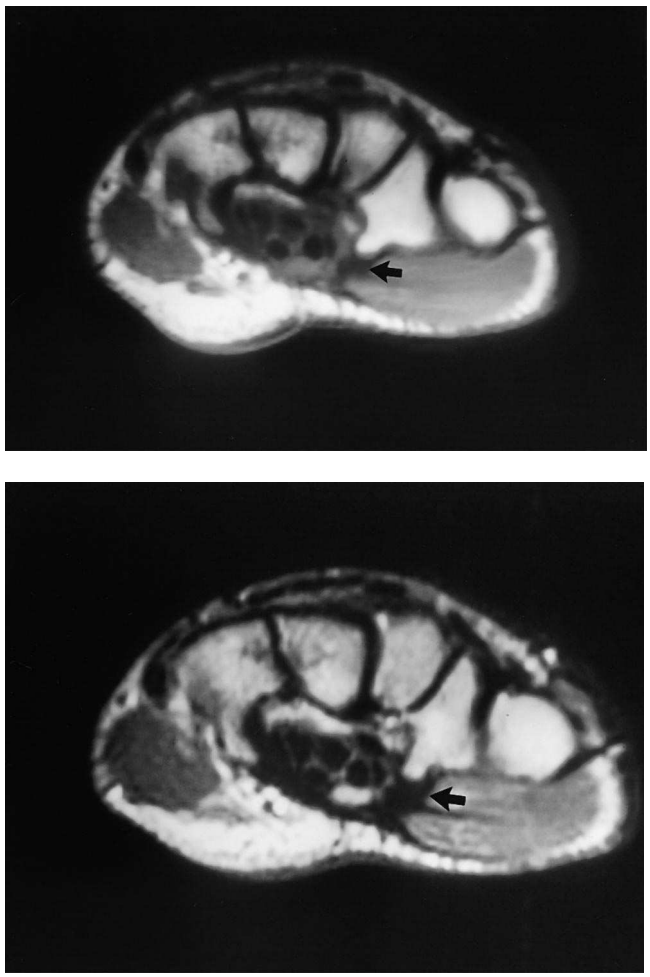

Fig. 29. Scarring and reattachment of the flexor retinaculum in a symptomatic patient following carpal tunnel release. Axial proton density (Top) and T2-weighted (Bottom) MR images show an area of thickening of low signal intensity adjacent to the triquetrum consistent with scarring (arrows). On the T2-weighted image (Bottom), the flexor retinaculum is seen spanning the floor of the carpal tunnel without interruption [From Chan W, Lang P, Genant H. MRI of the musculoskeletal system. Philadelphia, PA: Saunders, 1994. p. 228. With permission].

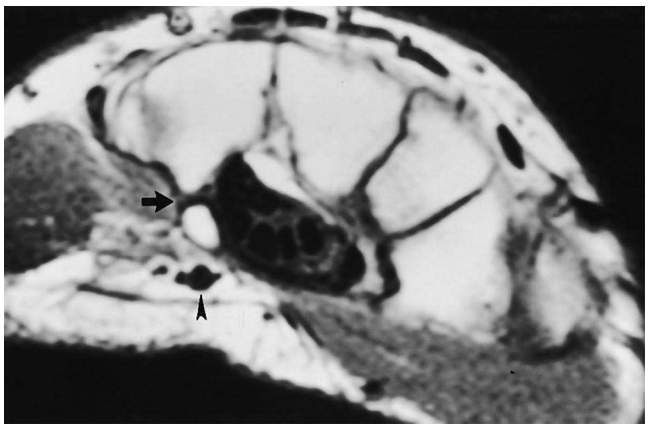

Fig. 30. Congenital lack of fusion of the hook of the hamate to the hamate predisposes this patient to Guyon's canal syndrome. Axial T1-weighted image demonstrates the synchondrosis between the hook and the hamate (arrow). Guyon's canal lies volar to the hook (arrowhead).

metacarpals, hook of the hamate (which can also have an unfused ossification center) (Fig. 30), and pisiform [58–63]. MRI can reliably demonstrate surrounding masses as well as anomalous muscles.

10. Synovial abnormalities

Effusions, inflammation, and edema are well seen by MRI, displaying signal intensities characteristic of fluid (long T1 and T2). Progression or improvement of synovitis can be monitored by MRI, allowing for presurgical evaluation and assessment of therapy. Characteristics of synovitis by MRI include irregular synovium that can be thickened with long-standing arthritis. It can be difficult to distinguish joint effusion from hypervascular pannus without the aid of dynamic gradient echo or spin-echo imaging following administration of an intravascular contrast agent such as gadolinium [64–66] (Fig. 31). Using dynamic sequential MRI immediately following gadolinium administration, one can differentiate inflamed synovium, which takes up the gadolinium within 30 s from synovial fluid, which does not enhance during the first 10 min following injection (Fig.

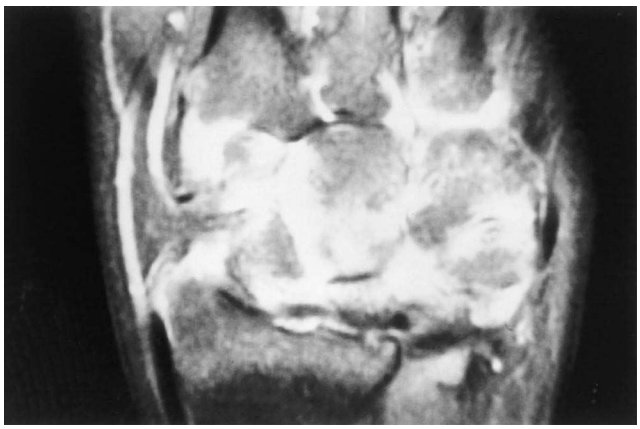

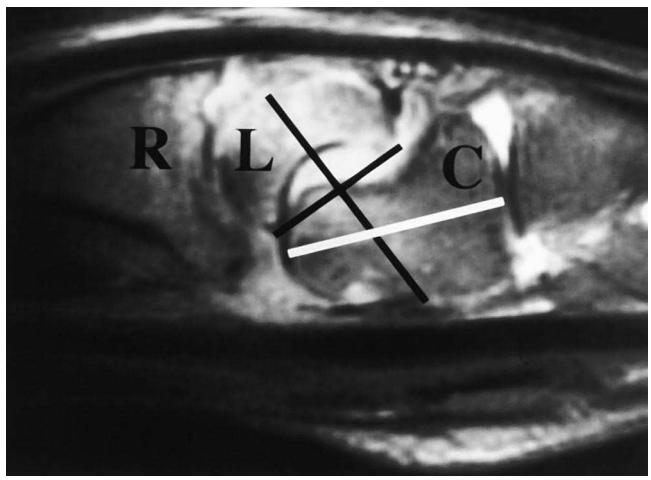

Fig. 31. (Top) Coronal fast spin-echo slice with fat suppression shows bright signal in wrist joint that could be large effusion or synovitis. Erosion of radius (curved open arrow) suggests synovitis. (Left) Gadolinium-enhanced coronal T1-weighted spin echo image with fat suppression shows diffuse enhancement of synovium in patient with fungal septic arthritis. (Right) Gadolinium-enhanced sagittal T1-weighted spin-echo image with fat suppression shows volar intercalated segment instability (VISI deformity) with palmar flexion of lunate (L) (long black line) compared to long axis of capitate (C) (white line). VISI deformity is frequently seen with inflammatory arthritidies.

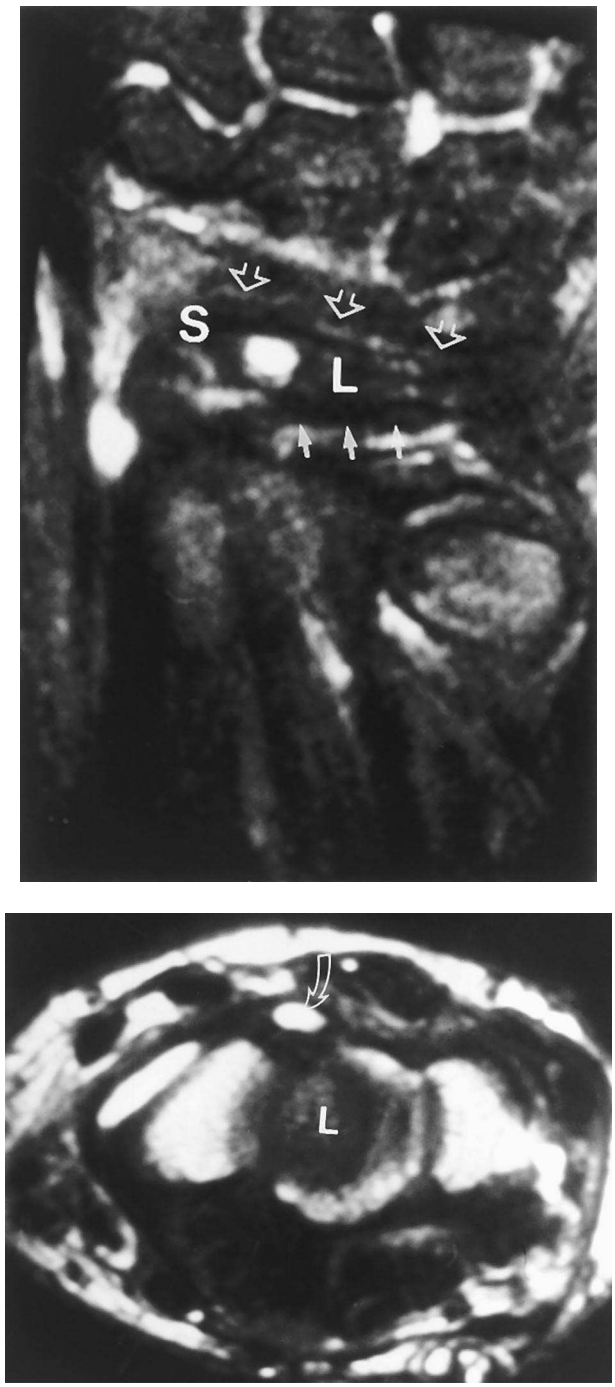

Fig. 32. (Top) Coronal fast spin-echo T2-weighted image with fat suppression shows bright signal of occult dorsal ganglion located above scapholunate ligament between radiotriquetral ligament (closed arrows) and dorsal intercarpal ligament (open arrows). S = scaphoid, L = lunate. (Bottom) Axial fast spin echo image without fat suppression shows dorsal carpal ganglion (curved arrow) located dorsal to scapholunate ligament. L = lunate.

31). In our experience, chronically thickened, fibrotic pannus has a shorter T2 relaxation time than synovial fluid, demonstrating intermediate to low signal intensity on T2-weighted MR images. Pannus may extend into the prestyloid recess and DRUJ, causing erosion of these structures.

MRI shows involvement of the dorsal tendon sheath and tendons with tenosynovitis and tendon rupture secondary to rheumatoid arthritis when such abnormalities are not clinically apparent [50]. MRI is also useful for the early identification of osseous and cartilaginous erosion in joints affected by inflammatory arthritis such as rheumatoid arthritis [67].

11. Benign soft tissue masses

Benign tumors occur much more frequently than malignant tumors in the wrist and hand [68]. MRI is useful for identifying and demonstrating the osseous and soft tissue extent of tumors in the wrist and hand [58,69,70]. The common benign soft tissue tumors of the wrist and hand include ganglion, giant cell tumor of the tendon sheath, lipoma, neural tumors, and hemangiomas [56,58,69–73].

Ganglia are the most common wrist mass (Fig. 32). In most patients, a diagnosis of a ganglion is made by clinical exam and by transillumination of the fluid-filled mass. Other patients present with wrist pain of uncertain etiology and may be referred for MR to rule out Kienböck's disease. Ganglia begin as evaginations of the capsule between the capsular ligaments. They are filled with mucinous fluid and may wax and wane in size. Eventually, some ganglia will become sequestered and will no longer drain freely. When they are symptomatic, it is usually because of mass effect. Most symptomatic ganglions traverse the dorsal wrist capsule overlying the interface between the scaphoid, lunate, and capitate bones although they are also frequently seen along the volar base of the radial styloid process. Small dorsal carpal ganglions are frequently seen in patients with central wrist pain and no other visible etiology. Most of these ganglia will be 4–5 mm in size and may have a visible stalk connecting it to the wrist joint. They can be clinically occult and may cause compression on neighboring structures [74]. MRI is useful for identifying an etiology for the

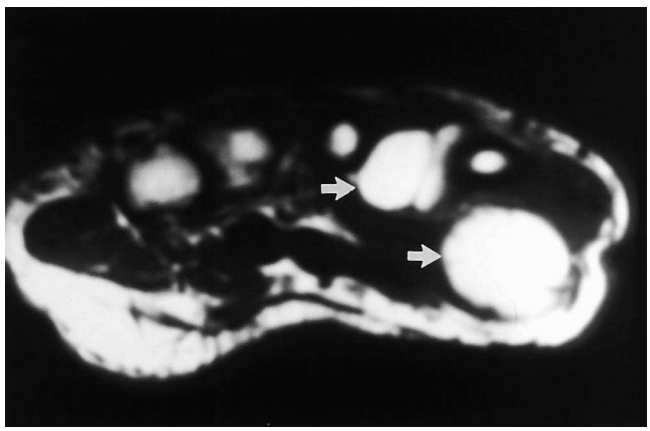

Fig. 33. Axial T1-weighted image shows lobulated intramuscular mass in thenar musculature (arrows) (mass has two lobes with few thin septations and follows fat signal on all imaging sequences).

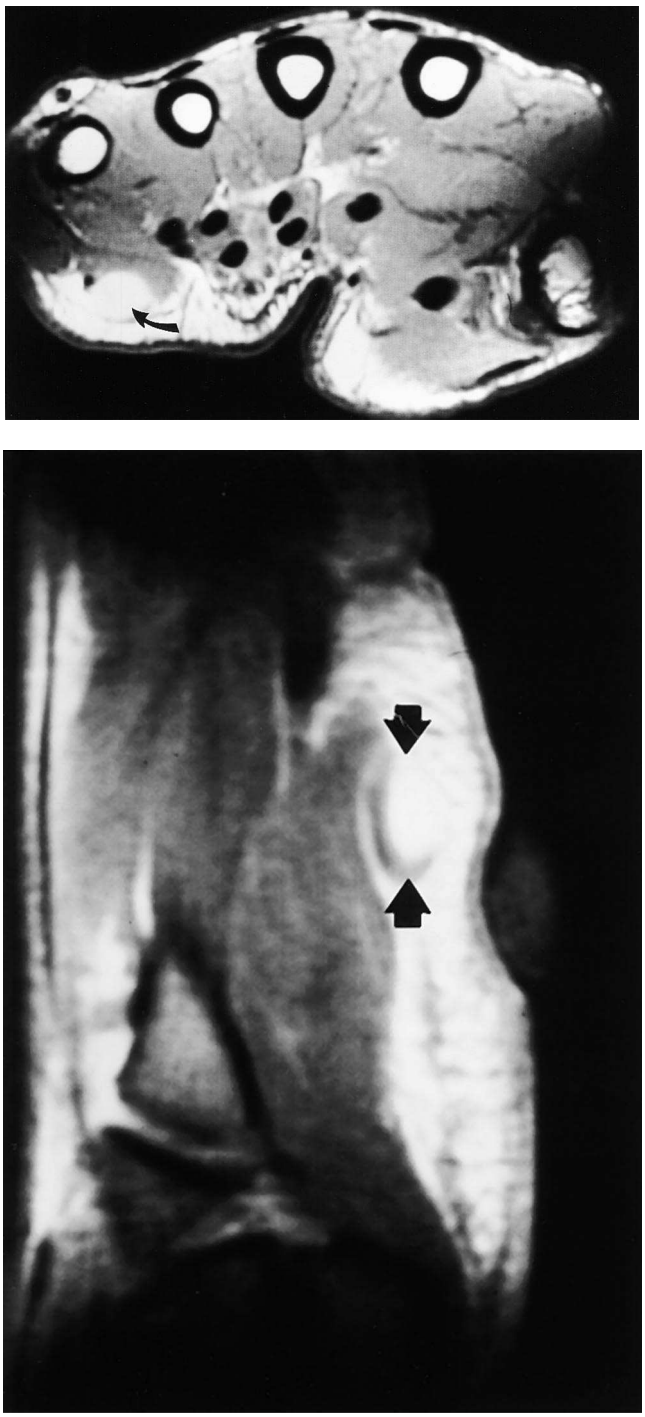

Fig. 34. (Top) Gadolinium-enhanced T1-weighted image with fat suppression shows neurofibroma (curved arrow) of superficial branch of ulnar nerve. Mass is located in hypothenar muscles and is well-circumscribed. (Bottom) Sagittal gadolinium-enhanced image with fat suppression shows enhancing neurofibroma in same patient with positive Tinel's sign.

patient's pain and for preoperative planning if surgical resection is contemplated. The surgeon must ligate the stalk of the ganglion to prevent a recurrence and would like to know the location and orientation of the stalk and the proximity of important neurovascular structures. Ganglia may be multiple and multiloculated. They contain mucinous material that has a long T1 and T2 relaxation time, similar to fluid. Differentiation from other benign lesions is not always possible based on MRI features alone. In some problematic cases, the addition of gadolinium enhancement will confirm that the mass is fluid-filled and not a solid mass.

Intramuscular lipomas are commonly located in the thenar or hypothenar eminences and have signal characteristics identical to subcutaneous fat (Fig. 33). They may contain streaks of low signal intensity (muscle fibers or septations) and are usually well circumscribed. Lipomas and ganglia, as well as other masses, can cause compression of the ulnar nerve in Guyon's canal along the ulnovolar aspect of the wrist [75,76].

Neural tumors such as neurofibromas and schwannomas are usually well-defined and isointense or slightly greater in signal intensity than muscle on T1-weighted MR images (Fig. 34). They may have homogeneous or heterogeneously increased signal on T2-weighted images [77]. The target

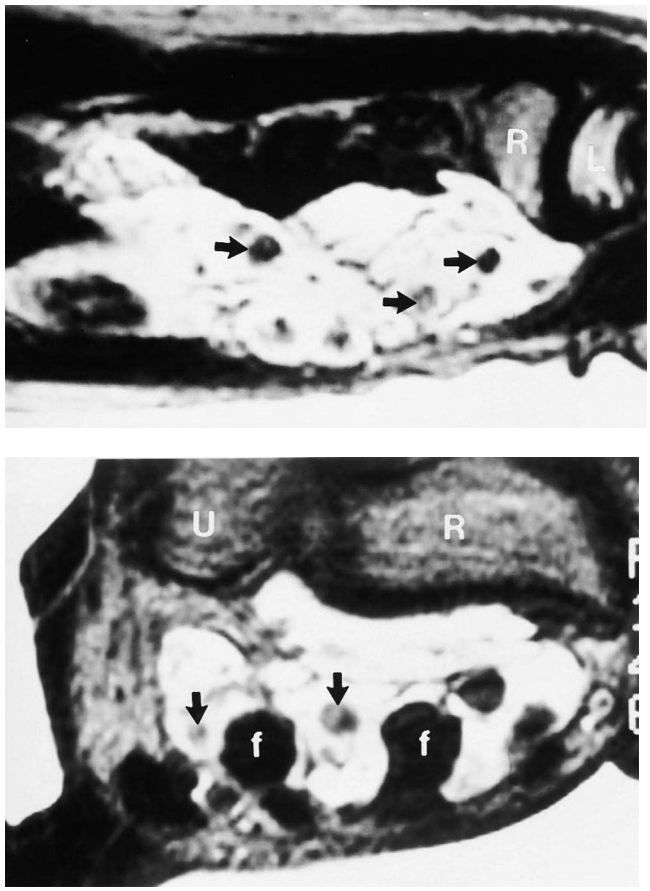

Fig. 35. (Top) Sagittal fast spin-echo T2-weighted image with fat suppression shows bright signal hemangioma in volar musculature with multiple rounded phleboliths (arrows). MR is useful for staging vascular lesions for surgical resection or ablational therapy. Bright signal outside forearm is water bag used to improve homogeneity of fat suppression. (Bottom) Axial fast spin-echo T2-weighted image shows bright signal of hemangioma surrounding flexor tendons (f). Multiple phleboliths are clue to diagnosis as vascular lesion, likely hemangioma. R = radius, U = ulna.

sign is a useful sign of neural lesion with peripheral bright signal and central intermediate to low signal on T2 or T2* images. Most nerve sheath tumors enhance intensely. The diagnosis may be suggested clinically by the presence of a Tinel's sign over the nerve.

Hemangiomas vary in composition and imaging characteristics (Fig. 35). Cavernous hemangiomas may have large fluid-filled components whereas some capillary hemangiomas may have a nonspecific imaging appearance. Most hemangiomas are isointense with muscle using T1WI but many hemangiomas contain a fatty component that may be easily identified using the T1WI. Most hemangiomas have a characteristic appearance on T2WI [78]. Multiple tubules are visible with bright signal intensity. Occasionally, phleboliths are visible in the mass. Gadolinium enhancement may be useful to identify solid from cystic components and may assist in preoperative planning of the margins when surgical resection is contemplated. Some hemangiomas may develop focal hemorrhages and the patient may present with an enlarging, painful mass. MRI at this time will show hematoma with complex signal characteristics (areas of bright and dark T1 and T2 signal intensity). In this setting, it may be reasonable to repeat the study in several weeks to determine if the mass has resolved.

MRI is also useful for identification of a variety of foreign bodies in the wrist and hand [79]. This is particularly true of nonradioopaque foreign bodies such as plastic and wood, which are not well seen with xeroradiography. Ultrasound can also be used for localization. Metallic foreign bodies produce some artifact, particularly on high field MR imagers.

References

[1] Smith DK. Dorsal carpal ligaments of the wrist: normal appearance on multiplanar reconstructions of three-dimensional fourier transform MR imaging. Am J Roentgenol 1993;161:119–25.

[2] Smith DK. Volar carpal ligaments of the wrist: normal appearance on multiplanar reconstructions of three-dimensional fourier transform MR imaging. Am J Roentgenol 1993;161:353–7.

[3] Totterman SMS, Miller R, Wasserman B, Blebea JS, Rubens DJ. Intrinsic and extrinsic carpal ligaments: evaluation by three-dimensional fourier transform MR imaging. Am J Roentgenol 1993;160:117–23.

[4] Smith DK. MR imaging of normal and injured wrist ligaments. MRI Clin North Am 1995;3:229–48.

[5] Levinsohn EM, Rosen ID, Palmer AK. Wrist arthrography: value of the three-compartmental injection method. Radiology 1991;179:231–9.

[6] Smith DK. Scapholunate interosseous ligament of the wrist: MR appearances in asymptomatic volunteers and arthrographically normal wrists. Radiology 1994;192:217–21.

[7] Smith DK, Snearly WN. Lunotriquetral interosseous ligament of the wrist: MR apperances in asymptomatic volunteers and arthrographically normal wrists. Radiology 1994;191:199–202.

[8] Kang HS, Kindynis P, Brahme SK, et al. Triangular fibrocartilage and intercarpal ligaments of the wrist: MR imaging-cadaveric study with gross pathologic and histologic correlation. Radiology 1991;181:401.

[9] Zlatkin MB, Chao PC, Osterman AL, et al. Chronic wrist pain: evaluation with high-resolution MR imaging. Radiology 1989;173:723.

[10] Schweitzer ME, Brahme SK, Hodler J, et al. Chronic wrist pain: spin-echo and short tau inversion recovery MR imaging and conventional and MR arthrography. Radiology 1992;182:205.

[11] Smith DK. MR arthrography of the wrist using iodinated contrast. Am J Roentgenol 1994;162:153.

[12] Shellock FG, Mandelbaum BP. Kinematic MR imaging of the joints. In: Mink JH, Deutsch AL, editors. MRI of the musculoskeletal system — a teaching file. New York: Raven Press, 1990.

[13] Bowers WH. The distal radioulnar joint. In: Green DP, editor. Operative hand surgery. 2nd ed. New York, NY: Churchill Livingstone, 1988.

[14] Taleisnick J. Pain on the ulnar side of the wrist. In: Taleisnik J, editor. Management of wrist problems, Vol. 1. Philadelphia, PA: Saunders, 1987.

[15] Palmer AK, Werner FW. The triangular fibrocartilage complex of the wrist: anatomy and function. J Hand Surg 1981;6:153.

[16] Mikic ZD. Age changes in the triangular fibrocartilage of the wrist joint. J Anat 1978;126:367.

[17] Palmer AK. Triangular fibrocartilage complex lesions: a classification. J Hand Surg 1989;14A:594.

[18] Harrison MO, Freiberger RH, Ranawat CS. Arthrography of the rheumatoid wrist joint. Am J Roentgenol 1971;112:480.

[19] Kessler I, Silberman Z. Experimental study of the radiocarpal joint by arthrography. Surg Gynecol Obstet 1961;112:33.

[20] Baker LL, Hajek PC, Bjorkengren A, et al. High-resolution magnetic resonance imaging of the wrist: normal anatomy. Skeletal Radiol 1987;16:128–32.

[21] Cerofolini E, Luchetti R, Pederzini L, et al. MR evaluation of the triangular fibrocartilage complex tears in the wrist: comparison with arthrography and arthroscopy. J Comput Assist Tomogr 1990;14:963.

[22] Golimbu CN, Firooznia H, Melone CP, et al. Tears of the triangular fibrocartilage of the wrist: MR imaging. Radiology 1989;173:731.

[23] Gundry CR, Kursunoglu-Brahme S, Schwaighofer B, Kang HS, Sartoris CJ, Resnick D. Is MR better than arthrography for evaluating the ligaments of the wrist? In vitro study. Am J Roentgenol 1990;154:337.

[24] Heuck A, Steinbach L, Neumann C, et al. Moglichkeiten der MR-tomographie bei erkrankungen von hand und handgelenk. Radiologe 1989;29:53.

[25] Reuther G, Erlemann R, Grunert J, Peters PE. Untersuchungstechnik und ligamentare binnenmorphologie in der MRT des handgelenks. Radiologe 1990;30:373.

[26] Beltra J, Noto AM, Mosure JC, Bools JD, Zuelzer WA, Christoforidis AJ. Meniscal tears: MR demonstration of experimentally produced injuries. Radiology 1986;158:691.

[27] Reicher MA, Hartzman S, Duckwiler GR, Basset LW, Anderson LJ, Gold RH. Meniscal injuries: detection using MR imaging. Radiology 1986;159:753.

[28] Sugimoto H, Shinozaki T, Ohsawa T. Triangular fibrocartilage in asymptomatic subjects: investigation of abnormal MR signal intensity. Radiology 1994;191:193–7.

[29] Wechsler RJ, Wehbe MA, Rifkin MD, et al. Computed tomogrphy diagnosis of distal radioulnar subluxation. Skeletal Radiol 1987;16:1.

[30] Staron RB, Feldman F, Haramati N, Singson RD, Rosenwasser M, Esser PD. Abnormal geometry of the distal radioulnar joint: MR findings. Skeletal Radiol 1994;23:369–72.

[31] Yao L, Lee JK. Occult intraosseous fracture: detection with MR imaging. Radiology 1988;167:749.

[32] Lee JK, Yao L. Stress fractures: MR imaging. Radiology 1988;169:217.

[33] O'Rahilly R. A survey of carpal and tarsal anomalies. J Bone Jt Surg 1953;35A:626.

[34] Reinus WR, Conway WF, Totty WG, et al. Carpal avascular necrosis: MR imaging. Radiology 1986;160:689.

[35] Cooney WP, Linscheid RL, Dobyns JH. Scaphoid fractures: problems associated with nonunion and avascular necrosis. Orthop Clin North Am 1981;15:381.

[36] Trumble TE. Avascular necrosis after scaphoid fracture: a correlation of magnetic resonance imaging and histology. J Hand Surg 1990; 15A:557.
[37] Preiser G. Einetypische posttraumatische und zur spontanfraktur fuhrende ostitis de naviculare carpi. Fortschr Geb Roentgenstr Nuklearmed 1910;15:189.
[38] Bray TJ, McCarroll HR. Preiser's disease: a case report. J Hand Surg [Am] 1984;9:730.
[39] Ekerot L, Eiken O. Idiopathic avascular necrosis of the scaphoid. Case report. Scand J Plast Reconstr Surg 1981;15:69.
[40] Allen PR. Idiopathic avascular necrosis of the scaphoid. A report of two cases. J Bone Jt Surg [Br] 1983;65:333.
[41] Hulten O. Uber anatomische variationen der Handgelenkknochen. Acta Radiol Scand 1928;9:155.
[42] Linscheid R. Ulnar lengthening and shortening. In: Taleisnik J, editor. Management of wrist problems. Hand clinics. Philadelphia, PA: Saunders, 1987;III:69.
[43] Lichtman DM. Kienböck's disease. The wrist and its disorders. In: Philadelphia, PA: Saunders, 1988.
[44] Alexander AH, Lichtman DM. Kienböck's disease. Orthop Clin North Am 1986;17:461.
[45] Amadio PC, Hanssen AD, Berquist TH. The genesis of Kienböck's disease: early diagnosis by magnetic resonance imaging. J Hand Surg 1987;12A:1044.
[46] Sowa DT, Holder LE, Patt PG. Application of magnetic resonance imaging to ischemic necrosis of the lunate. J Hand Surg 1989; 14A:1008.
[47] Pennes DR, Louis DS, Fechner K. Bone marrow imaging (letter to the editor). Radiology 1989;170:894.
[48] Erickson SJ, Cox IH, Hyde JS, Carrera GF, Strandt JA, Estkowski LD. Effect of tendon orientation on MR imaging signal intensity: a manifestation of the "magic angle" phenomenon. Radiology 1991; 181:389.
[49] Beltran J, Mosure JC. Magnetic resonance imaging of tendons. Crit Rev Diagn Imaging 1990;30:111.
[50] Rubens DJ, Blebea JS, Totterman SMS, Hooper MM. Rheumatoid arthritis: evaluation of wrist extensor tendons with clinical examination versus MR imaging — a preliminary report. Radiology 1993;187: 831–8.
[51] Mesgarzadeh M, Schneck CD, Bonakdarpour A, et al. Carpal tunnel: MR imaging: Part II. Carpal tunnel syndrome. Radiology 1989; 171:749.
[52] Sunderland S. Carpal tunnel syndrome. Nerves and nerve injuries. 2nd ed. New York: Livingstone, 1981.
[53] Mesgarzadeh M, Schneck CI, Bonakdarpour A. Carpal tunnel: MR imaging: Part I. Normal anatomy. Radiology 1989;171:743.
[54] Middleton WD, Kneeland JB, Kellman GM, et al. MR imaging of the carpal tunnel: normal anatomy and preliminary findings in the carpal tunnel syndrome. Am J Roentgenol 1987;148:307.
[55] Zeiss J, Skie M, Ebraheim N, et al. Anatomic relations between the median nerve and flexor tendons in the carpal tunnel: MR evaluation in normal volunteers. Am J Roentgenol 1989;153:533.
[56] Weiss KL, Beltran J, Lubbers LM. High field MR surface coil imaging of the hand and wrist: Part II. Pathologic correlations and clinical relevance. Radiology 1986;160:147.
[57] Sugimoto H, Miyaji N, Ohsawa T. Carpal tunnel syndrome: evaluation of median nerve circulation with dynamic contrast-enhanced MR imaging. Radiology 1994;190:459–66.
[58] Binkovitz LA, Cahill DR, Ehman RL, et al. Magnetic resonance imaging of the wrist: normal cross sectional imaging and selected abnormal cases. RadioGraphics 1988;8:1171.
[59] Zeiss J, Jakab E, Khimji T, Imbriglia J. The ulnar tunnel at the wrist (Guyon's canal): normal MR anatomy and variants. Am J Roentgenol 1992;158:1081.
[60] Carlson CS, Clark GL. False aneurysm of ulnar artery in Guyon's canal. J Hand Surg [Am] 1983;8:223.
[61] Guliani G, Poppi M, Pozzati E, Forti A. Ulnar neuropathy due to a carpal ganglion: the diagnostic contribution of CT. Neurology 1990; 40:1001.
[62] Subin GD, Mallon WJ, Urbaniak JR. Diagnosis of ganglion in Guyon's canal by magnetic resonance imaging. J Hand Surg [Am] 1989;14:640.
[63] Zahrawi F. Acute compression ulnar neuropathy at Guyon's canal resulting from lipoma. J Hand Surg [Am] 1984;9:238.
[64] Konig H, Sieper J, Wolf KJ. Rheumatoid arthritis: evaluation of hypervascular and fibrous pannus with dynamic MR imaging enhanced with Gd-DTPA. Radiology 1990;176:473.
[65] Kursunoglu-Brahme S, Riccio T, Weisman MH, et al. Rheumatoid knee: role of gadopentetate-enhanced MR imaging. Radiology 1990;176:831.
[66] Reiser MF, Bongartz GP, Erlemann R, et al. Gadolinium-DTPA in rheumatoid arthritis and related diseases: first results with dynamic magnetic resonance imaging. Skeletal Radiol 1989;18:591.
[67] Rominger MB, Bernreuter WK, Kenney PJ, Morgan SL, Blackburn WD, Alarcon GS. MR imaging of the hands in early rheumatoid arthritis: preliminary results. RadioGraphics 1993;13:37–46.
[68] Butler ED, Hamell JP, Seipel RS, deLorimier AA. Tumors of the hand. A 10-year survey and report of 437 cases. Am J Surg 1960; 100:293.
[69] Steinbach LS. Tumors and synovial processes in the wrist and hand. In: Reicher MA, Kellerhouse LE, editors. MRI of the wrist and hand. New York: Raven Press, 1990.
[70] Miller TT, Potter HG, McCormack RR. Benign soft tissue masses of the wrist and hand: MRI appearances. Skeletal Radiol 1994;23: 327–32.
[71] Karasick D, Karasick S. Giant cell tumor of tendon sheath: spectrum of radiologic findings. Skeletal Radiol 1992;21:219.
[72] Miller TT, Potter HG, McCormack RR. Benign soft tissue masses of the wrist and hand: MRI appearances. Skeletal Radiol 1994;23: 327–32.
[73] Binkowitz LA, Berquist TH, McLeod RA. Masses of the hand and wrist: detection and characterization with MR imaging. Am J Roentgenol 1990;154:323.
[74] Cardinal E, Buckwalter KA, Braunstein EM, Min AD. Occult dorsal carpal ganglion: comparison of ultrasound and MR imaging. Radiology 1994;193:259–62.
[75] Angelides AC. Ganglions of the hand and wrist. In: Green DP, editor. Operative hand surgery. 2nd ed. New York: Churchill Livingstone, 1988.
[76] Bogumill GP. Tumors of the wrist. In: Lichtman DM, editor. The wrist and its disorders. Philadelphia, PA: Saunders, 1988.
[77] Kransdorf MJ, Jelinek JS, Moser RP, et al. Soft-tissue masses: diagnosis using MR imaging. Am J Roentgenol 1989;153:541–7.
[78] Buetow PC, Kransdorf MJ, Moser RP, Jelinek JS, Berrey BH. Radiologic appearance of intramuscular hemangioma with emphasis on MR imaging. Am J Roentgenol 1990;154:563–7.
[79] Russell RC, Williamson DA, Sullivan JW, Suchy H, Suliman O. Detection of foreign bodies in the hand. J Hand Surg 1991;16A:2.